NASA CONTRACTOR REPORT

NASA CR-135105

FATIGUE CRACK GROWTH AT ELEVATED TEMPERATURE 316 STAINLESS STEEL AND H-13 STEEL

by

Wen-Ching Chen

and

H. W. Liu

Syracuse University

Syracuse, New York 13210

for

NATIONAL AERONAUTICS AND SPACE ADMINISTRATION, WASHINGTON, D.C. 1977

TECHNICAL REPORT

FATIGUE CRACK GROWTH AT ELEVATED TEMPERATURE

316 STAINLESS STEEL AND H-13 STEEL

by

Wen-Ching Chen

H. W. Liu

Sponsored by:

NATIONAL AERONUATICS AND SPACE ADMINISTRATION

NASA Grant No.: NGR 33-022-157

George Sachs Fracture and Fatigue Research Laboratory
Syracuse University
Department of Chemical Engineering and Materials Science
Syracuse, New York 13210

MTS-HWL-4116-776

ACKNOWLEDGEMENT

The authors are indebted to the National Aeronautics and Space Administration for sponsoring this research program through Contract No. NASA-NGR-33-022-157. The authors also wish to thank Mr. C. Chave for his laboratory assistance, Mr. H. Turner for her typing of this manuscript and Mr. R. Ziemer for his drawing of the graphs.

ABSTRACT

High temperature fatigue is one of the most complex material problems. It is well known that creep deformation and cyclic plastic deformation are quite different in their mechanisms. The damages caused by these two deformation processes also differ significantly. Based on this observation, the concept of strainrange partitioning analysis on the combined effects of fatigue and creep was proposed.

Crack growths were measured at elevated temperatures under four types of loading: pp, pc, cp, and cc. In H-13 steel, all these four types of loading gave nearly the same crack growth rates, and the length of hold time had negligible effects. In AISI 316 stainless steel, the hold time effects on crack growth rate were negligible if the loading was tension-tension type; however, these effects were significant in reversed bending load, and the crack growth rates under these four types of loading varied considerably. Both tensile and compressive hold times caused increased crack growth rate, but the compressive hold period was more deleterious than the tensile one.

Metallographic examination showed that all the crack paths under different types of loading were largely transgranular for both CTS tension-tension specimens and SEN reversed cantilever bending specimens. In addition, an electric potential technique was used to monitor crack growth at elevated temperature. The optimum positions for current leads and potential probes were determined.

I. INTRODUCTION

The principles of linear-elastic fracture mechanics have been successfully applied in characterizing the propagation of fatigue cracks in austenitic stainless steels at elevated temperatures by Brothers (1), James (2), and Shahinian (3). As long as the average stress in the net section remains generally elastic, the crack growth rate, da/dN, is governed by the crack tip stress intensity factor range, ΔK , at elevated temperatures. At room temperature, there is no significant effect of cyclic frequency and loading wave form on fatigue crack growth rate. However, the creep effect, the environmental effect (most possibly, oxidation), as well as the mechanical properties of the materials themselves strongly enhance the crack growth rate at elevated temperatures. In dealing with the fatigue-creep interaction, we are generally concerned with the observation that fatigue at elevated temperatures is subject to time effects, i.e., frequency, hold time, loading wave form, and environment.

An increase in temperature generally increases the crack growth rate for a given ΔK and reduces the threshold ΔK for crack growth. (2,3) Speidel (4) indicated that the increase of cycle-dependent fatigue crack growth rate accompanied by an increase in temperature correlated with the corresponding decrease of the Young's modulus. Wei (5) suggested that, for a given ΔK, an Arrhenius type equation might describe the fatigue crack growth rate at eleveated temperatures.

$$da/dN = A\, f(\Delta K)\, \exp \frac{-u(\Delta K)}{kT} \qquad (1)$$

where A is a constant; f(ΔK), the crack driving force; u(ΔK), the apparent activation energy, k = Boltzmann's constant, and T = absolute temperature. However, James et al. (2) and Shahinian et al. (3) have shown that the crack growth rate data of both AISI 304 stainless steel for the temperature range of 75° to 1200°F and the data of AISI 316 stainless steel for the temperature range of 70° to 1100°F, respectively, did not conform to a single Arrhenius type relationship. Since fatigue crack growth at elevated temperatures obviously is a thermally-activated process, they conclude that more than one thermally-activated process is dominant in fatigue cracking over the entire temperature range, and a more complete definition of the pre-exponential term, A is needed.

James (6) found that in the plot of log (da/dN) vs. log (ΔK) for various frequencies, there existed a critical value of ΔK, beyond which the crack growth rate increased with decreasing frequency, and below which there existed a frequency independency of crack growth. In their log-log plots of crack growth rate, da/dN, vs. frequency ν, Ohmura et al. (7) and Solomon et al. (8) showed that at the high frequency extreme there was a frequency-independent and purely cycle-dependent transgranular crack growth mode; whereas, at the low frequency extreme, there was a purely time-dependent intergranular crack growth mode. In the transition region between these two extremes, the crack growth was of mixed cracking modes and was of weak frequency-dependency.

Generally, the longer the hold time the faster will be the cyclic rate of crack growth. However, Mowbray et al. (9) showed that the precipitation of a new metallurgical phase reduced the crack growth rate as the hold time exceeded a critical value. Therefore, the metallurgical instabilities must be also dealt with in analyzing the effects of

hold time.

It is still not clear whether the environmental effect or the creep effect decisively influences the fatigue crack growth rate at elevated temperatures. Both environmental and creep effects are time-dependent. The most possible environmental effects at elevated temperatures are caused by oxidation. The strain-enhanced oxide near a crack tip could either advantageously or detrimentally modify the crack propagation. (10)

The effects of temperature, frequency, hold time and environment on crack growth rate at elevated temperature have been investigated; however, the effects of loading wave form are yet to be studied.

Fatigue crack growth at elevated temperatures is complicated. In addition to cyclic plastic deformation, creep deformation and creep damage become important when the test temperature is above one half of the absolute melting point of the material. When a machine component or a structural member is cyclically loaded at elevated temperatures, both cyclic plastic deformation and creep deformation might have occurred. Cyclic plastic deformation and creep deformation are inelastic deformation, but the mechanisms and the damages caused by these two types of inelastic deformation are quite different. Cyclic plastic deformation takes place in slip bands which are distributed throughout the grains, and therefore, causes transgranular cracking; whereas, the creep deformation is generally caused by diffusion controlled mechanisms and grain boundary sliding and migration, and therefore, intergranular cracking often occurs. At elevated temperatures, fatigue cracks are generally initiated along grain boundaries, but crack propagation might be either transgranular or intergranular However, as test temperature, hold time and mean stress are increased, and cyclic loading frequency is reduced,

creep deformation and creep cracking are favoured, and thus tendency for intergranular crack propagation is increased. (11)

Because of the differences in the mechanisms and the damage processes, these two types of inelastic deformation bore different relationships to failure life at elevated temperatures. These basic differences in mechanisms, damage processes, and thus, in the relationships between failure life and the time-independent cyclic plastic deformation and the time-dependent creep deformation, lead to the concept of strainrange partitioning analysis.(12,13,14,15) The imposed inelastic strain is separated into four different types, i.e., $\Delta\varepsilon_{pp}$, $\Delta\varepsilon_{pc}$, $\Delta\varepsilon_{cp}$ and $\Delta\varepsilon_{cc}$, each of which bore a different relation to failure life. If the loading-unloading is rapid enough to preclude the creep-effect at elevated temperatures, and no hold period is introduced to the cycle, the imposed inelastic strain is $\Delta\varepsilon_{pp}$-completely reversed cyclic plasticity. With rapid loading-unloading and the hold period at tensile peak in between, the imposed inelastic strain is defined as $\Delta\varepsilon_{cp}$-tensile creep reversed by compressive cyclic plasticity; while the hold time is at the compression peak, it is $\Delta\varepsilon_{pc}$-tensile cyclic plasticity reversed by compresive creep. When the hold periods are introduced at both the tensile and compressive peaks, with rapid loading and unloading, the imposed inelastic strain is $\Delta\varepsilon_{cc}$-completely reversed creep. The low cycle fatigue experimental data at elevated temperatures show that the failure lives under these four types of cyclic straining are quite different.

The overall objective of this investigation was to analyze fatigue crack growth at elevated temperatures in terms of creep damage and the damage caused by cyclic plastic deformation. The effects of cyclic frequency and loading wave form on crack growth rate at elevated temperature were studied.

II. EXPERIMENTAL PROCEDURE

Fatigue crack growth in AISI 316 stainless steel at 1300°F and in H-13 steel at 1100°F was studied. The chemical compositions of these two materials are given in Table 1. The stainless steel specimens were tested in as-received condition. The heat-treatment schedule for H-13 steel is given in Table 2.

Both tension-tension type and reversed bending type of loading were employed. The tension-tension type tests were conducted on compact tension (CTS) specimens and were load controlled. The single-edge-notched (SEN) specimens were tested under completely reversed displacement controlled cantilever bending. Fig. 1 shows the experimental set-up for the reversed bending test. Fig. 2 shows the specimen geometries. The cyclic displacement was ± 0.5 mm. Initially, the load range was 900 lbs. (± 450 lbs.) or 4000 newtons (± 2000 newtons). As the crack grew, the range gradually decreased to 700 lbs. (3114 newtons), with compressive maximum slightly higher (approximately 20% higher) than the tensile maximum. This could have been caused by crack closure in the compressive side. Only tension-tension type of tests were conducted on H-13 steel.

The overall objective of this investigation was to analyze fatigue crack growth at elevated temperature in terms of creep deformation and cyclic plastic deformation. Four different types of loading wave forms, i.e., pp, pc, cp, and cc, as shown in Figs. 3 and 4, were applied. In the above notation, p represents cyclic plastic deformation and c represents creep deformation; the first letter refers to the type of deformation imposed by the tensile half of the cycle, and the second letter refers to the type of deformation imposed at the compressive half of the cycle.

Hold time at either the maximum or the minimum load was used to induce creep deformation. The period of hold time varied from 2.7 to 60 seconds. Frequencies from 0.9 to 500 cpm were used.

Measurements of crack length were made through the glass window of the resistance furnace by means of a travelling microscope mounted onto a stationary rack. An electric potential technique was also used for crack length measurements. The circuit diagram is shown in Fig. 5. The potential probes and the current leads inside the furnace were 0.040 in. (0.1 cm) diameter, chromel wire; whereas, those outside of the furnace were copper wire. The potential probes and the current leads were spot-welded to the specimen. The potential drop across the crack was taken as the difference between the readings when the power supply was on and off. Thus, the thermal EMF's generated between the potential probes and the testpiece at the testing temperature were eliminated. A constant current of 5A was used for all tests, and the potential drop was measured with an accuracy of 1 μV. Extensive calibration was done, and an overall accuracy of ± 0.003" (± 0.008 cm) in crack length measurements was achieved. The potential drop and the maximum and the minimum loads were recorded periodically.

The crack closure under reversed bending was also studied by the electric potential technique. Metallographic examination on crack paths under different types of cyclic loading was also made.

III. CALIBRATION FOR THE ELECTRIC POTENTIAL TECHNIQUE FOR CRACK LENGTH MEASUREMENT

The electric potential technique has been successfully used for monitoring crack growth at room temperature. (16,17,18) This technique was adapted for crack length measurements at elevated temperatures. Fig. 5 shows the circuit diagram. The results of the calibration are given in Figs. 6 and 7. The crack extension A/A_o is related to the potential drop V/V_o, where A_o is the starter notch length; A, A_o plus the crack extension; V_o, the initial potential drop across the starter notch without crack extension; and V, the potential drop across the starter notch plus the crack extension. For a given planar specimen geometry, the result of the calibration is independent of specimen thickness, heat-treatment, test temperature, and material resistivity and chemical composition.

The potential drop across the crack was very sensitive to the positioning of the potential probes and the current leads. The optimum positions for the potential probes and the current leads for high reproducibility of the calibration curve are illustrated in Ref.17 for both CTS and SEN specimens by means of an analogue method. The current leads were situated far apart from the notch, and the potential probes were on the top face of the specimen as close to the open end of the notch as possible, as shown in Fig. 8. With this knowledge of the equi-potential distributions on these two types of specimen, the optimum positions for current leads and potential probes could be easily determined by detecting the variations of potential drop across the crack caused by the change in the distance between the current leads or between the potential probes or both.

The effects of the positioning of the current leads and the potential probes on the potential drop across the crack for the CTS specimen are shown in Fig. 9. The potential drop across the crack remained unchanged if the potential probes were located within 1/8" (0.3 cm) from the notch surfaces. Also, positioning the current leads further apart lowered the potential gradient near the starter notch. As a result of these findings, the current leads were located on the top face of the specimen far apart from the notch and the potential probes were positioned on the top face of the specimen as close as possible to the notch slot. Similarly, for the SEN specimens, the current leads were at the ends of the specimen, and the potential probes were on the top face of the specimen as close as possible to the notch. In this investigation, the calibration was made by using actual specimens and extending the crack by fatigue cycling.

Although this technique had been employed at room temperature, the temperature fluctuation in the furnace generates additional thermal EMF, which has to be compensated in order to achieve a high degree of accuracy for the crack length calibration. A dummy specimen was used, which was connected in series to the testpiece, Fig. 5. The dummy specimen was of the same size, geometry and material as the testpiece, and was ketp uncracked in the same furnace. At the same furnace temperature it can be assumed that the potential drops, measured from both testpiece and dummy specimen V_1' and V_{o2}' are affected to the same extent, i.e., $V_1' = n \cdot V_1$ and $V_{o2}' = n \cdot V_{o2}$, where n is the multiplying factor caused by the temperature change, and V_1 and V_{o2} are the potential drops across the crack in the testpiece and across the starter notch

in the dummy specimen at the prescribed test temperature. Let V_1'/V_{o2}' be the ratio of the potential drop measured from the testpiece to the potential drop measured from the dummy specimen at the time of crack extension measurement; and V_{o1}/V_{o2}, the ratio of the potential drop measured from the testpiece to the potential drop measured from the dummy specimen at the beginning of the test without crack extension in the testpiece. These two quantities, V_1'/V_{o2}' and V_{o1}/V_{o2}, are measured, and the ratio of the potential drops due to crack extension alone, which excludes the temperature effects is

$$V/V_o = \frac{V_1'/V_{o2}'}{V_{o1}/V_{o2}} = V_1/V_{o1} \quad . \tag{2}$$

The effects of these variables caused by temperature fluctuation were thus eliminated.

With the technique described above, the calibration showed a very good reproducibility, and an accuracy of ± 0.003" (± 0.008 cm), for crack growth monitoring, was achieved.

IV. RESULTS AND DISCUSSION

The bulk of the test program was conducted on AISI 316 stainless steel. The results of the cyclic crack growth under the reversed bending tests are summarized in Figs. 10, 11 and 12. The specimen was 2" (5.08 cm) wide with a machined notch crack starter 0.4" (1.02 cm) deep. The loading was displacement controlled. Five different types of loading were tested. The loading wave form and the hold time are noted in the figures. In these figures Δa is the crack extension from the notch root.

As shown in Fig. 10, the average crack growth rate under ramp loading at low cyclic frequency (10 cpm) was more than 10 times faster than that under rapid ramp loading (100 cpm). The hold time at compression, pc loading, was more deleterious than the hold time at tension, i.e., cp loading. The crack growth rate varied from 2×10^{-6} inches/cycle (5×10^{-6} cm/cycle) to 6×10^{-5} inches/cycle (1.5×10^{-4} cm/cycle). One specimen, solid points in Fig. 11, was first tested under the pc type loading. When Δa reached 0.3" (0.762 cm), the loading was changed to cp type. The data, i.e., the solid points, agreed well with the data of the earlier tests. The reproducibility of the test data was found to be very good. The results of a similar test showed very good reproducibility of the data under the cc type loading and the low frequency ramp loading (10 cpm), Fig. 12.

A set of compact tension specimen was used to test the tension-tension type of loading. The results are shown in Figs. 13, 14, and 15, and are summarized in Fig. 16. The hold times used were 4, 15, and 60 seconds. The loading and unloading rates were the same for all of these

specimens, with the exception of the ramp loading at 100 cpm. These tests were load controlled. The cyclic load range was 400 to 4000 lbs. (1780 to 17800 newtons). The load range was too high to apply the linear elastic fracture mechanics. The loading level of these specimens was higher than the bending specimens, and consequently, the crack growth rates: 1×10^{-4} to 5×10^{-4} inches/cycle (2.5×10^{-4} to 1.3×10^{-3} cm/cycle), were much higher. The effects of cc, pc and cp types of tension-tension loading were much smaller than the effects of reversed bending load. The crack growth rates under cc, pc and cp types of loading were nearly the same; moreover, they were twice as fast as the crack growth rate under ramp fatigue loading at 100 cpm. The effects of hold time on cyclic crack growth rate were very small. The crack growth rate at 10 cpm ramp loading was only 30% higher than the growth rate under ramp fatigue loading at 100 cpm. This was in great contrast to the results of the reversed bending tests as shown earlier, where the crack growth rate at 10 cpm ramp loading was nearly 10 times faster than the ramp fatigue loading at 100 cpm.

Fig. 17 shows the additional results under the tension-tension type of loading but at lower load levels: 200 - 2000 lbs. (890 - 8900 newtons) and 100 - 1000 lbs. (445 - 4450 newtons). Tests were conducted at 10 cpm and 100 cpm. As the load level was reduced, the frequency effect on crack growth rate gradually disappeared. The crack growth rate, da/dN, versus the stress intensity factor range, ΔK, was plotted in Fig. 18. The data showed that below $\Delta K = 20$ ksi$\sqrt{\text{in}}$ (22 MPa$\sqrt{\text{m}}$), the frequency effect disappeared. Above this ΔK level, the crack growth rate at 10 cpm ramp loading was approximately 30% higher than the ramp loading at 100 cpm. James (6) had found similar results.

Fig. 19 shows the data of two samples tested at 500 cpm ramp loading and 10 cpm "square" wave form loading. The loading and unloading rate of the low frequency sample was very close to that of the high frequency sample, 500 cpm. The load range was from 150 to 1500 lbs. (668 to 6680 newtons). It was interesting to find that the crack growth rates of these two samples were nearly the same.

The results of compact tension specimens under tension-tension type of cyclic loading are also plotted in Figs. 20 and 21. The number of cycles needed to grow a crack by 0.6" (1.524 cm) vs. the applied load range ΔP is plotted in Fig. 20; the total time needed to grow a crack by 0.6 " (1.524 cm) vs. the applied load range is plotted in Fig. 21. The solid squares are the results of "square" wave form loading at 10 cpm. These two plots showed that the crack growth rate had a strong cyclic dependency and that time effect was secondary. In other words, the creep effect was less than the fatigue effect. The results also indicated that an increase in the frequency increased the number of cycles to failure and decreased the time to failure.

In general, the hold time had a negligible effect if the loading was tension-tension type, but the effects of hold time were significant in reversed bending loading. In the later case, both tensile and compressive hold times increased the crack growth rate. It is reasonable to expect that creep and stress relaxation at tensile dwell period caused an increase in the crack growth rate. However, when a crack was under a compressive load, the surface was closed, and the crack lost its effect. It seemed that the hold time at compression caused creep and stress relaxation of the mating crack surfaces in contact. Soon after the loading was reversed, the mating surfaces separated from each other. Therefore, the effective applied stress intensity factor range was increased,

which caused faster crack growth rate.

Figs. 22, 23, 24, 25, and 26 show the metallographys along the crack paths of SEN reversed cantilever bending specimens under five different cyclic wave form loadings, i.e., ramp loading (10 cpm and 100 cpm), cp, pc and cc (10 cpm). These pictures were taken at the mid-section of the specimen. The metallographs on the side surfaces showed the same pattern. The cracks in these specimens were all grown by 0.6 inches (1.524 cm). Pictures near both the crack tips and the notch roots are shown. The crack growth data of these specimens are shown in Fig. 10. The maximum difference in crack growth rates among these specimens was more than 10 times. The crack paths were largely transgranular for all these five specimens in spite of the differences in their hold times and frequencies. Figs. 27, 28, 29, and 30 show the same results for the CTS tension-tension specimens. Considerable crack branching was observed for the 10 cpm ramp loading, which gave the fastest crack growth rate; the branching was the least for the 100 cpm ramp loading, which gave the lowest crack growth rate. The amount of branching decreased in the order of 10 cpm ramp loading, pc, cc, cp, and 100 cpm ramp loading, which paralleled the decreasing order of crack growth rates among these five types of loading wave form. The initiation sites of the crack branches were often located along the grain boundary; however, the crack paths were predominantly transgranular. An estimate of the portions of intergranular crack paths was made. The results were 15%, 11%, 11%, 8%, and 7% for the five types of loading, respectively. These estimates were not very accurate but they indicated the qualitative trend that the higher the percentage of intergranular cracking, the faster the crack growth rate. Moreover, this small difference in intergranular cracking should

not be the main cause for the wide difference in crack growth rate shown in Fig. 10. This observation was contrary to the finding of Manson et al. (12,13,14) indicating that the tensile creep in a high temperature fatigue test for a cp type of loading caused intergranular cracking. This discrepancy was probably due to the limited size of the region of high plastic strain range found in our cracked specimens, whereas the low cycle fatigue push-pull hour-glass cylindrical specimens underwent gross "uniform" plastic strain. It should also be noted that the hold times by Manson et al. were often more than one minute, but for these tests the hold times were limited to 6 seconds, which could have been too short to incur sufficient damage to cause intergranular cracking.

Cracks in two SEN specimens under reversed cantilever bending were grown by 0.3" (0.762 cm). The tracings of the load vs. the electric potential drop, which was a measure of crack length, were then recorded with an X-Y recorder as shown in Fig. 31a and 31b. These two specimens were under ramp loading but at different frequencies: 10 cpm, and 100 cpm. These two loading conditions give the fastest and the slowest crack growth rates as shown earlier in Fig. 10. The tracing for the 100 cpm frequency definitely indicated crack closure under the compressive loading. On the other hand, there was only a very slight indication, if any, of crack closure for the 10 cpm specimen.

When a crack is closed, it loses its effectiveness. Therefore, crack closure reduces the effective stress intensity factor range, and the crack growth rate is correspondingly reduced. However, this observation was only qualitative due to the limitation of the sensitivity of the instrument used, the uncertainty of the effect of oxides, and the

mismatch between the two mating crack surfaces. This observation of crack closure was also supported by the metallographic pictures of Figs. 22 through 26. The crack openings at both the notch root and the crack tip in Fig. 22 (ramp loading, 10 cpm) were definitely much wider than those in Fig. 26 (ramp loading, 100 cpm). The crack openings and the crack growth rates of the other three specimens were in between these two extremes. A wide crack opening delayed the crack closure during the unloading half cycle and promoted the crack opening during the loading half cycle. It, therefore, increased the effective load range and in turn, both the effective stress intensity factor range and the crack growth rate.

Possible reasons for the large differences in crack growth rates in 316 stainless steel SEN specimens under reversed cantilever bending are grain boundary damage caused by creep deformation, corrosion, crack tip geometric change caused by creep, and relaxation of the compressive stress between the mating crack surfaces during the compressive half cycle of the loading. Undoubtedly, each of these factors played a role in high temperature fatigue crack growth. Yet, the effects of grain boundary damage and corrosion were not the dominant ones. The metallographic pictures did not show extensive intergranular cracking. The crack paths were largely transgranular. The effect of corrosion for pc-type of loading should have been less than that for cp-type of loading. Yet, the crack growth rates showed otherwise. Thus, the results of this investigation indicated as possible explanations for the large differences in crack growth rates (shown in Fig. 10) the crack tip geometry change by creep and the stress relaxation between mating crack surfaces.

Fig. 32 shows the data of compact tension specimens on H-13 steel. The test temperature was 1100°F. The data showed negligible differences in crack growth rates under all four types of loading. Also, the difference in hold time at both maximum and minimum loads, 4 seconds and 16 seconds, has negligible effect on crack growth rate.

It was found that the types of loading cycles had significant effects on fatigue lives of unnotched cylindrical 316 stainless steel specimens, which were under cyclic push-pull strain controlled loading. (12,13,14,15) However, the effects of hold time on the fatigue lives of unnotched H-13 steel was negligible. (19) This observation on the difference of the sensitivities of 316 stainless steel and H-13 steel to fatigue-creep interaction agreed with our results on fatigue crack growth. However, our results showed that the compressive creep was more deleterious than the tensile one, and the effects of creep on cyclic crack growth rates were less than the effects on the lives of unnotched cylindrical specimens.

V. CONCLUSIONS

1. An electric potential technique for crack length measurement at elevated temperature was developed and an extensive calibration work was made. The optimum positions for current leads and potential probes were determined in order to achieve a high accuracy and good reproducibility. An accuracy of ±0.003" (± 0.008 cm) in crack length measurement was achieved.

2. In 316 stainless steel, the hold time effects were much less if the loading was tension-tension type in comparison with the reversed bending loading. Both tensile and compressive hold times caused an increase in crack growth rate, however, the compressive hold period was more deleterious than the tensile one.

3. In 316 stainless steel specimens under tension-tension type of loading within the limited range of hold time studied, the creep effect during the hold time is less than the fatigue effect.

4. In 316 stainless steel, there existed a transition value of ΔK, 20 Ksi$\sqrt{in}$ (22 MPa$\sqrt{in}$), in the plot of log (da/dN) vs. log (ΔK), below which the crack growth rate was independent of frequency, and beyond which decreasing the frequency increased the crack growth rate.

5. Metallographic examination on 316 stainless steel specimens showed that all the crack paths of different wave-form loadings were largely transgranular for both CTS tension-tension specimens and SEN reversed cantilever bending specimens.

6. There seemed to be a qualitative correlation between da/dN and crack opening displacement, COD. The COD was large and the da/dN fast for the 316 stainless steel specimen at 10 cpm ramp loading, the COD

was small and the da/dN slow for the 316 stainless steel specimen at 100 cpm ramp loading. There was also an indication of crack closure for the high frequency test. The wider crack opening in the case of 10 cpm ramp loading delayed the beginning of crack closure in the unloading half-cycle, and promoted the opening of the crack opening during the loading half-cycle. Hence, it increased the effective load range and the effective stress intensity factor range, and it enhanced crack growth rate.

7. In H-13 steel, the effects of hold time and loading wave form on crack growth rate were negligible.

REFERENCES

1. Brothers, A. J., "Fatigue Crack Growth in Nuclear Reactor Piping Steel", General Electric Report GEAP-5607, Mar., 1968.

2. James, L. A., and Schwenk, E. B. , "Fatigue-Crack Propagation of Type 304 Stainless Steel at Elevated Temperatures", Metallurgical Transaction, Vol. 2, No. 2, 1971, pp. 491-496.

3. Shahinian, P., Smith, H. H., and Watson, H. E., "Fatigue Crack Growth in Type 316 Stainless Steel at High Temperature", Journal of Engineering for Industry, Transaction, American Society of Mechanical Engineering, Vol. 93, No. 4, 1971, pp. 976-980.

4. Speidel, M. O., "Fatigue Crack Growth at High Temperature", in High-Temperature Materials in Gas Turbines, P. R. Sahm and M. O. Speidel ed., Elsevier Scientific Publishing Co., Amsterdam, Netherland, 1974, pp. 207-255.

5. Wei, R. P., "Fatigue-Crack Propagation in a High-Strength Aluminum Alloy", The International Journal of Fracture Mechanics, Vol. 4, No. 2, 1968, pp. 159-168.

6. James, L. A., "The Effect of Frequency upon the Fatigue-Crack Growth of Type 304 Stainless Steel at 1000°F", Stress Analysis and Growth of Crack, ASTM STP 513, American Society for Testing and Materials, 1972, pp. 218-229.

7. Ohmura, T., Pelloux, R. M., and Grant, N. J., "High Temperature Fatigue Crack Growth in a Cobalt Base Superalloy", Engineering Fracture Mechanics, Vol. 5, 1973, pp. 909-922.

8. Solomon, H. D., and Coffin, L. F., Jr., "Effects of Frequency and Environment on Fatigue Crack Growth in A286 at 1100°F", Fatigue at Elevated Temperature, ASTM STP 520, American Society for Testing and Materials, 1973, pp. 112-122.

9. Mowbray, D. F., and Woodford, D. A., "Observations and Interpretation of Crack Propagation Under Conditions of Transient Thermal Strain", International Conference on Creep and Fatigue in Elevated Temperature Applications, Institution of Mechanical Engineering, Sheffield, U.K., 1973.

10. Cook, R. H., and Skelton, R. P., "Environment-Dependence of the Mechanical Properties of Metals at High Temperature", International Metallurgical Review, Vol. 19, 1974, pp. 199-222.

11. Wells, C. H., Sullivan, C. P., and Gell, M., "Mechanisms of Fatigue in the Creep Range", Metal Fatigue Damage-Mechanism Detection, Avoidance, and Repair, ASTM STP 495, American Society for Testing and Materials, 1971, pp. 61-122.

12. Manson, S. S., Halford, G. R., and Hirschberg, M. H., "Creep-Fatigue Analysis by Strain-Range Partitioning", Symposium on Design for Elevated Temperature Environment, American Society of Mechanical Engineering, New York, 1971, pp. 12-24.

13. Manson, S. S., "The Challenge to Unify Treatment of High Temperature Fatigue - A Partisan Proposal Based on Strain-range Partitioning", Fatigue at Elevated Temperature, ASTM STP 520, 1973, pp. 744-782.

14. Halford, G. R., Hirschberg, M. H., and Manson, S. S., "Temperature Effects on the Strain-range Partitioning Approach for Creep Fatigue Analysis", Fatigue at Elevated Temperature, ASTM STP 520, 1973, pp. 658-669.

15. Manson, S. S., Halford, G. R. and Nachtigall, A. J., "Separation of the Strain Components for Use in Strain-range Partitioning", NASA TM X-71737, National Aeronautics and Space Administration, Cleveland, Ohio, 1975.

16. Anctil, A. A., Kuka, E. B., and DiCesare, E., "Electric Potential Technique for Determining Slow Crack Growth", Proceedings, American Society of Mechanical Engineering, Vol. 63, 1963, pp. 799-808.

17. Ritchie, R. O., Garrett, G. G., and Knott, J. F., "Crack Growth Monitoring: Optimization of the Electric Potential Technique Using an Analogue Method", International Journal of Fracture Mechanics, Vol. 7, 1971, pp. 462-467.

18. Sidey, D., "The Measurement of Crack Growth in Metals by the Electric Potential Method", Engineering Report, CUED/C-MAT/TR9, University of Cambridge, U.K.

19. Halford, G. R., "Discussion on Paper No. 6", Specialists Meeting on Low Cycle High Temperature Fatigue, AGARD-CP-155, North Atlantic Treaty Organization, 1974, p. 6-17.

TABLE 1

CHEMICAL COMPOSITIONS OF TYPE 316 STAINLESS STEEL AND H-13 STEEL

AISI Type 316 Stainless Steel (%)

C	Mn	Si	P	S	Cr	Ni	Mo	Fe
0.08	2.00	1.00	0.045	0.030	18.00	14.00	3.00	Balance

H-13 Steel (%)

C	Cr	Mn	V	Si	Mo	Fe
0.40	5.00	0.40	1.10	1.10	1.35	Balance

TABLE 2

HEAT-TREATMENT SCHEDULE FOR H-13 STEEL

1. Austenitizing by preheating the specimens to 1400°F for 1/2 hour, then holding at 1850°F for 1 hour, followed by air cooling to room temperature.
2. Double tempering at 1200°F for 2 hours. Air cooling to room temperature.

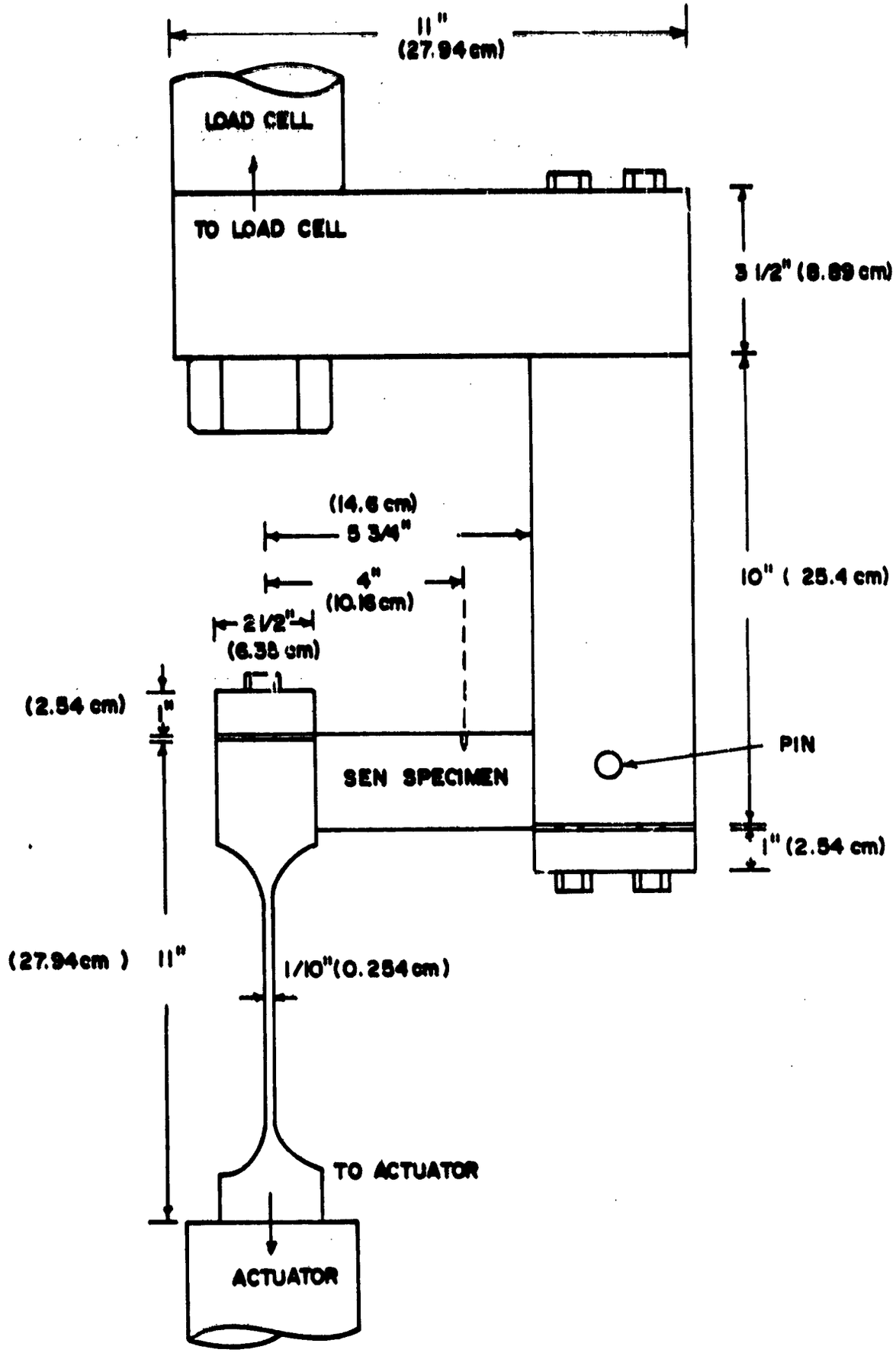

FIG. 1 EXPERIMENTAL SET-UP FOR CANTILEVER BENDING TEST.

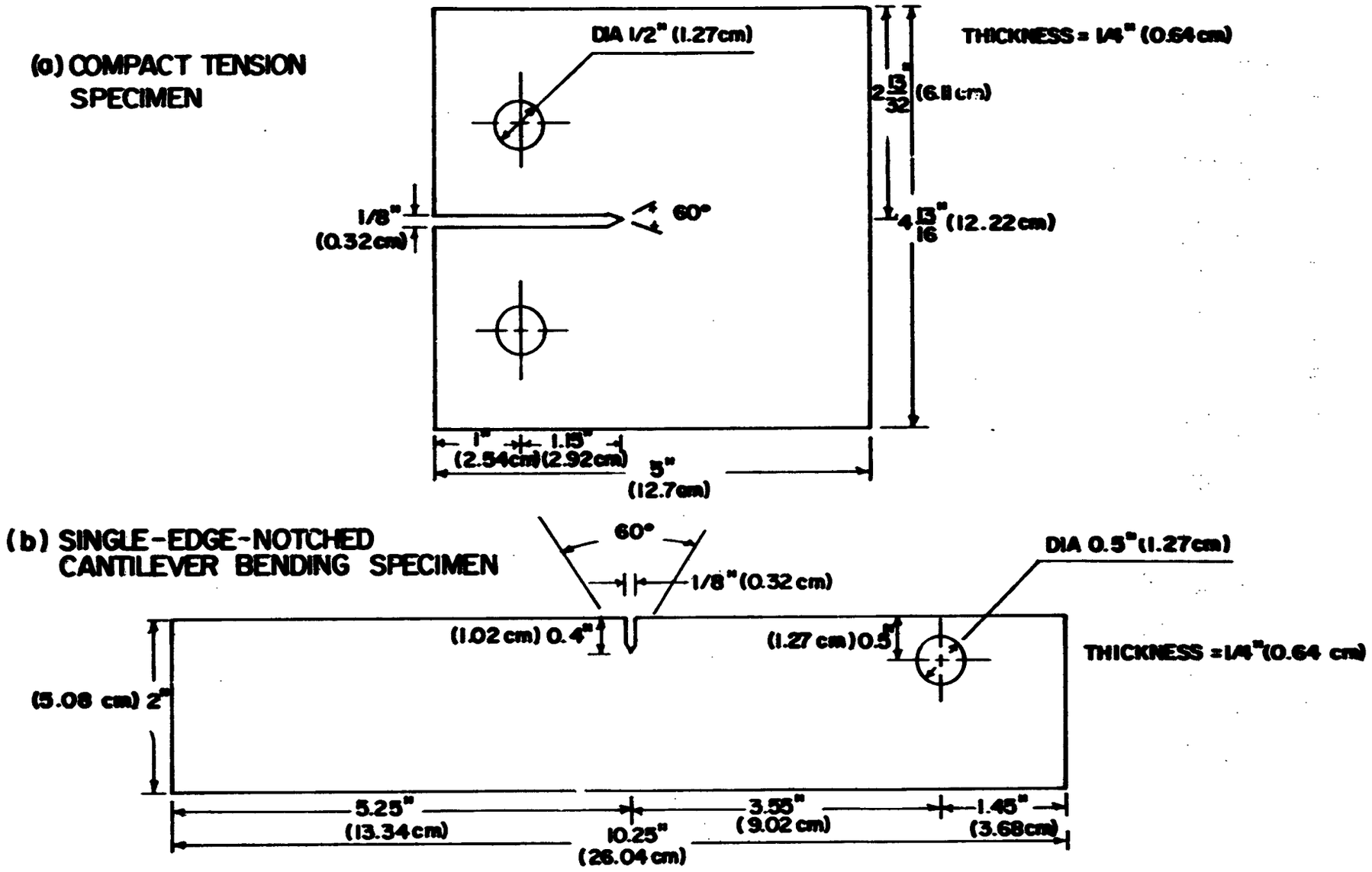

FIG. 2 COMPACT TENSION SPECIMEN (CTS) AND SINGLE-EDGE-NOTCHED (SEN) CANTILEVER BENDING SPECIMEN.

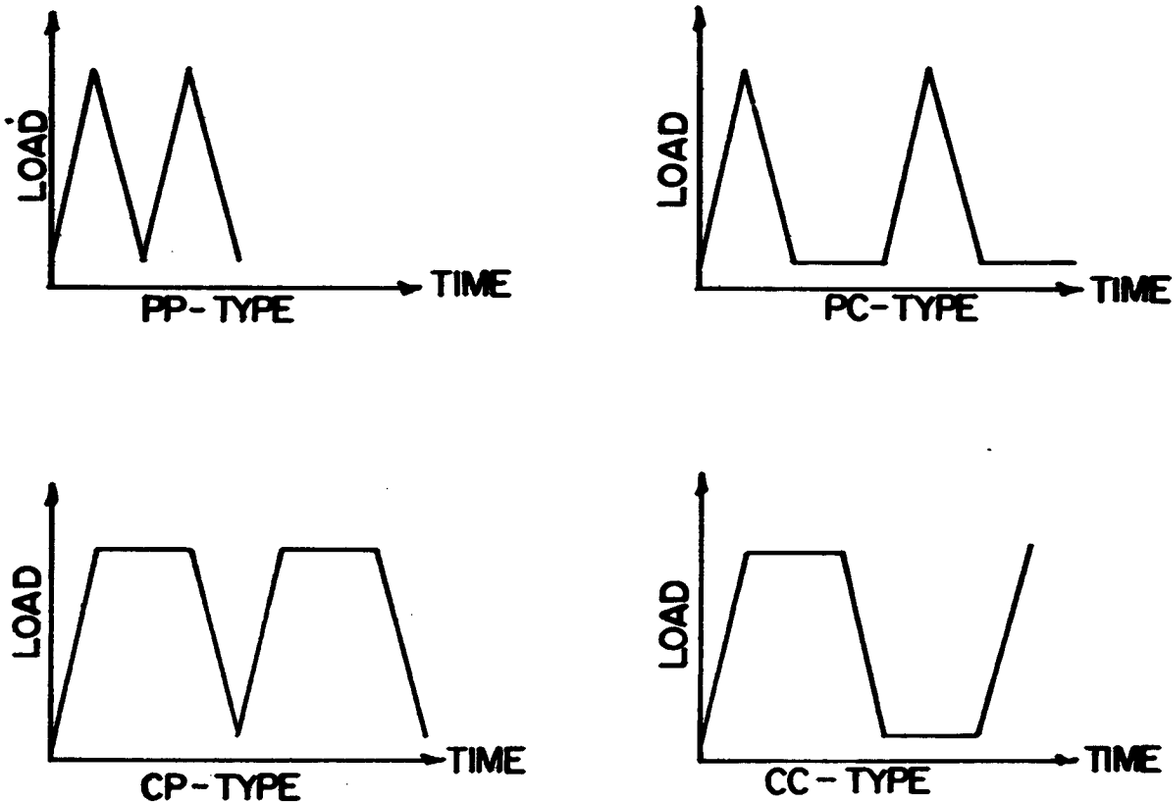

FIG. 3 CYCLIC LOADING WAVE FORMS FOR TENSION-TENSION TESTS.

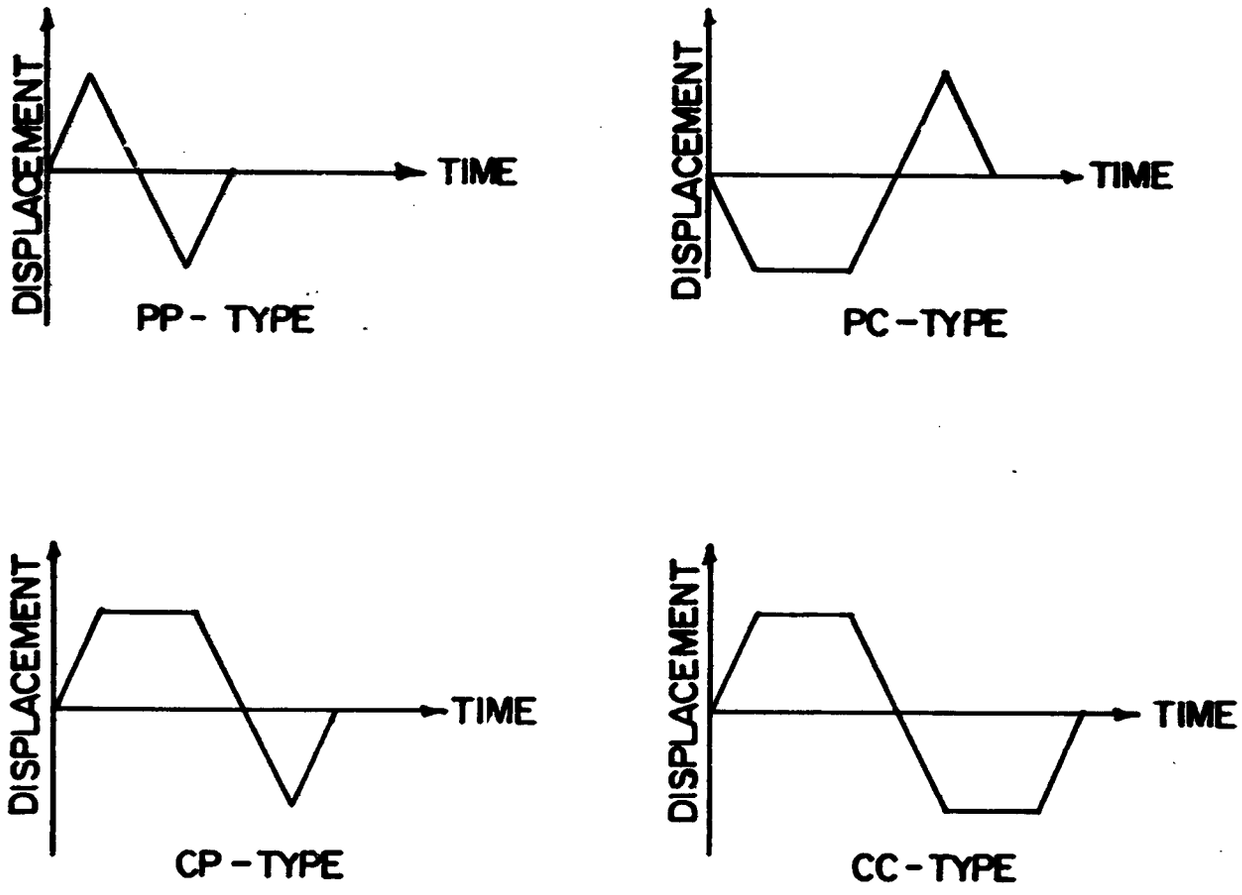

FIG. 4 CYCLIC LOADING WAVE FORMS FOR REVERSED CANTILEVER BENDING TESTS.

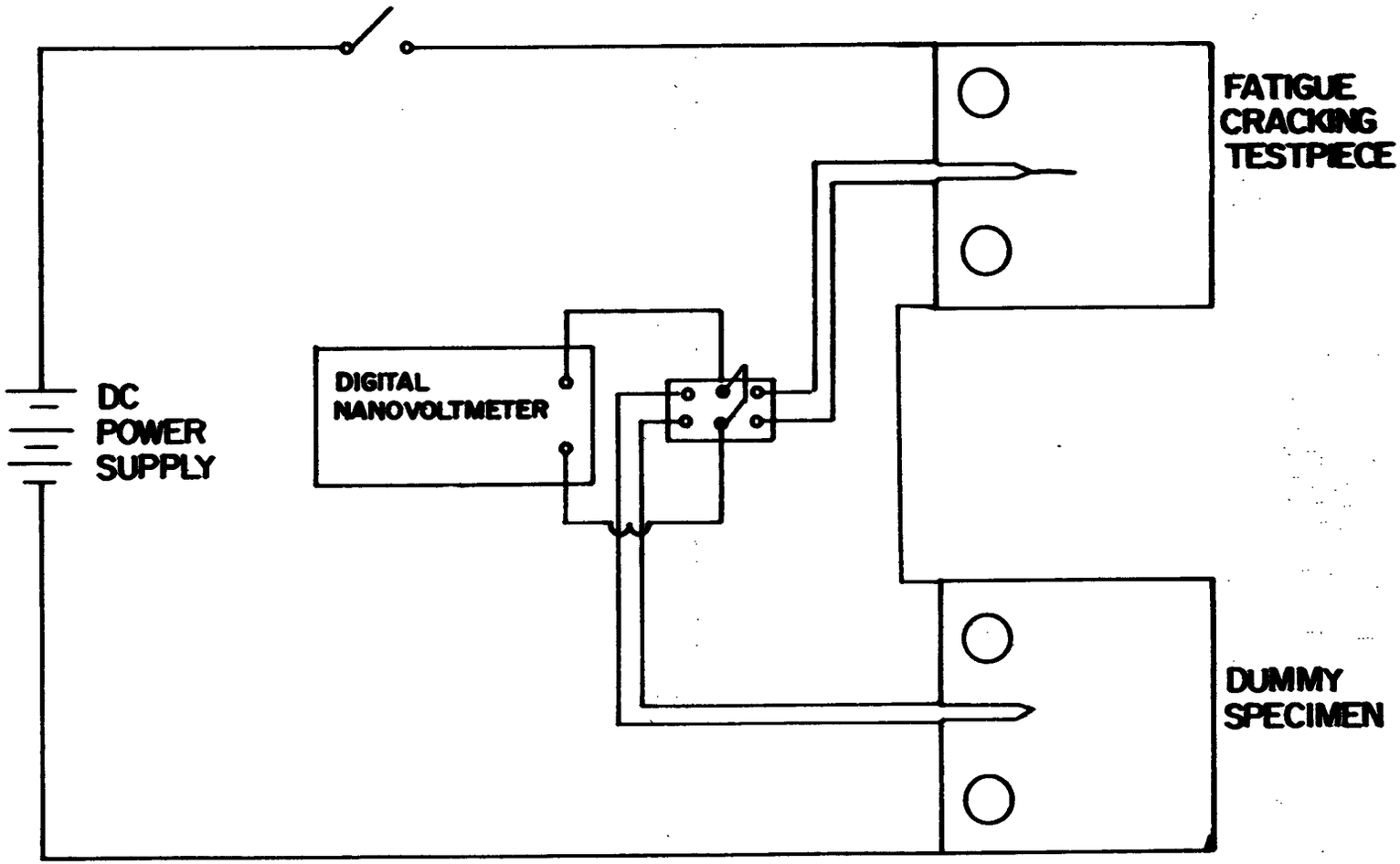

FIG. 5 SCHEMATIC DRAWING OF ELECTRIC POTENTIAL TECHNIQUE.

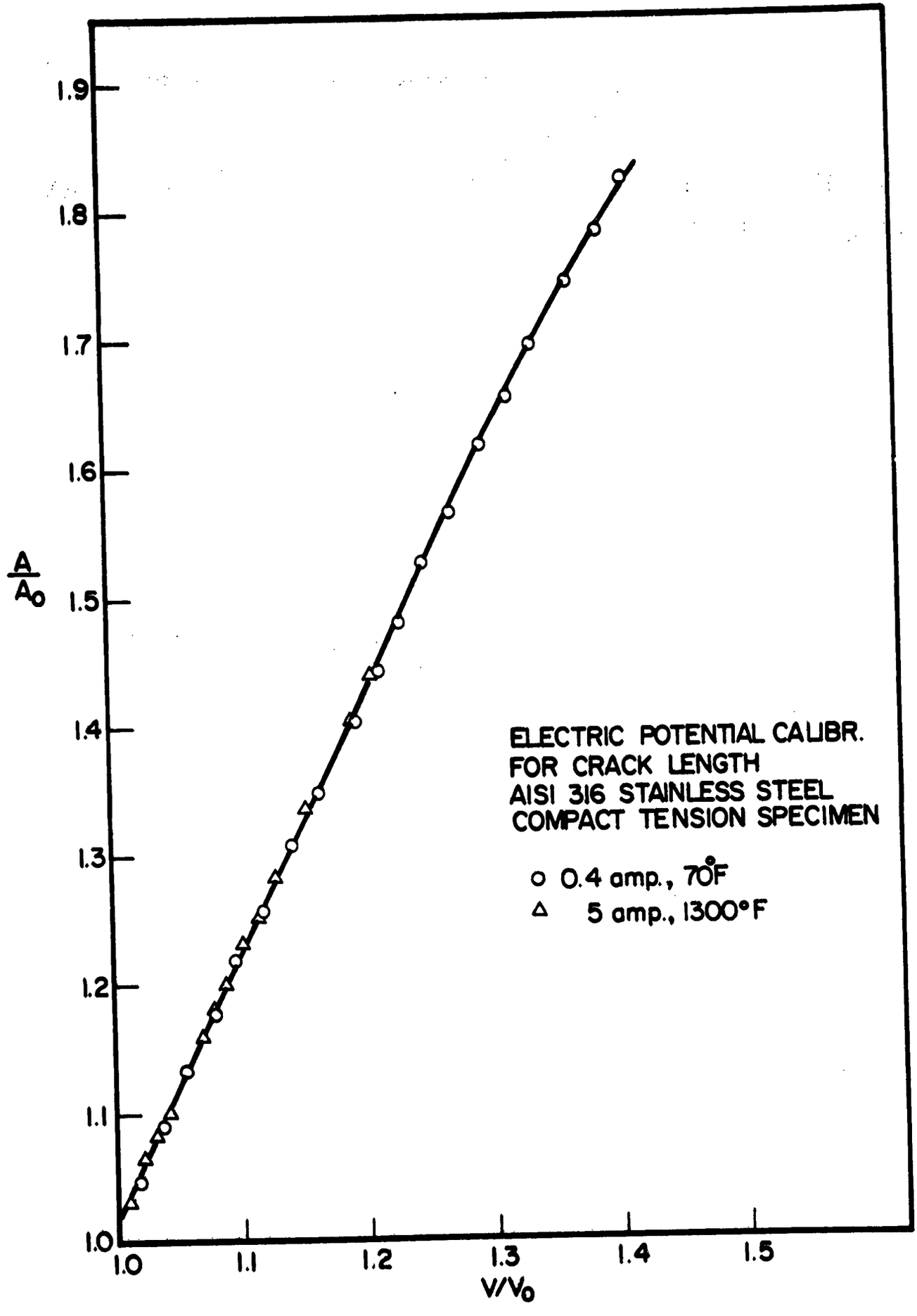

FIG. 6 ELECTRIC POTENTIAL CALIBRATION CURVE FOR 316 STAINLESS STEEL COMPACT TENSION SPECIMEN.

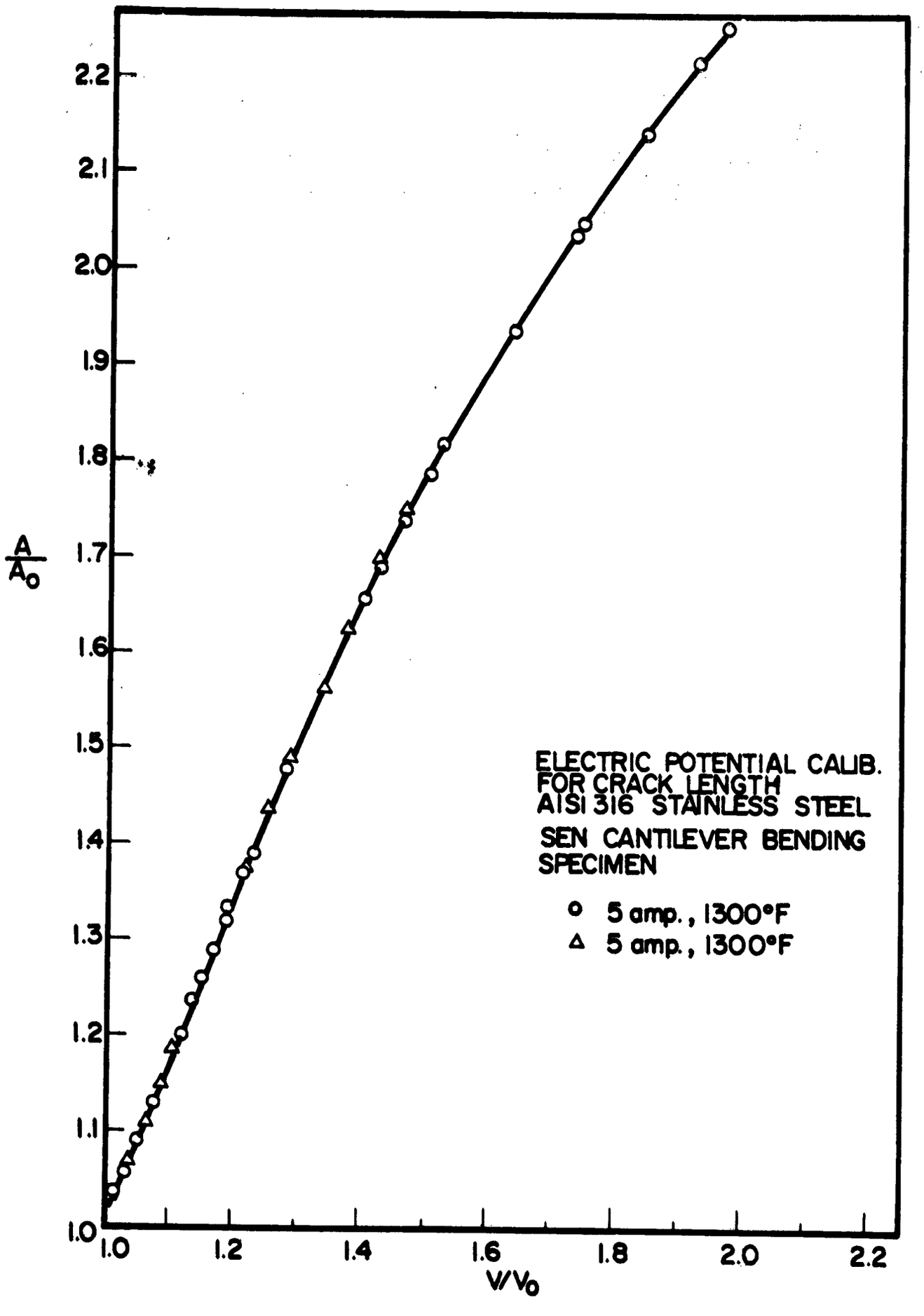

FIG. 7 ELECTRIC POTENTIAL CALIBRATION CURVE FOR 316 STAINLESS STEEL SEN CANTILEVER BENDING SPECIMEN.

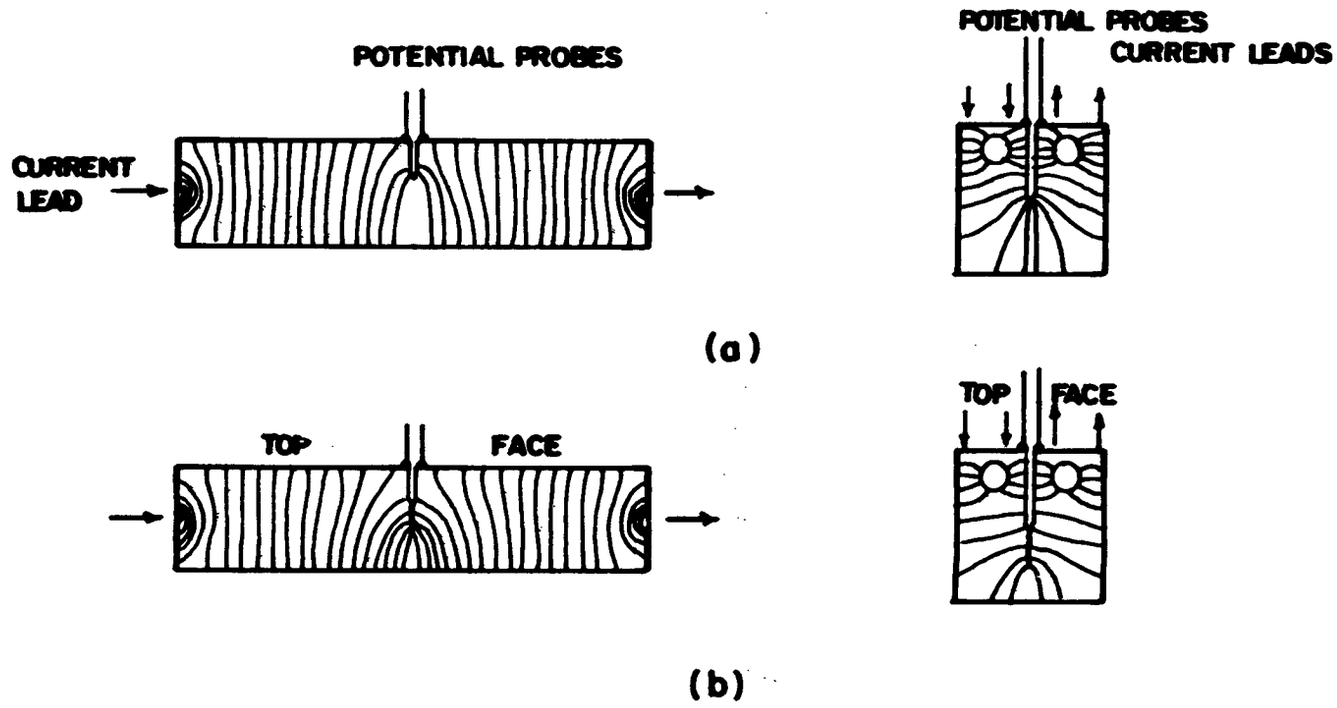

Fig. 8 Equi-potential distributions for SEN and CTS specimens in the "uniform current" configuration: (a) uncracked, (b) cracked (arrows indicate positions of current input and output). (From Ritchie et. al., ref. 17)

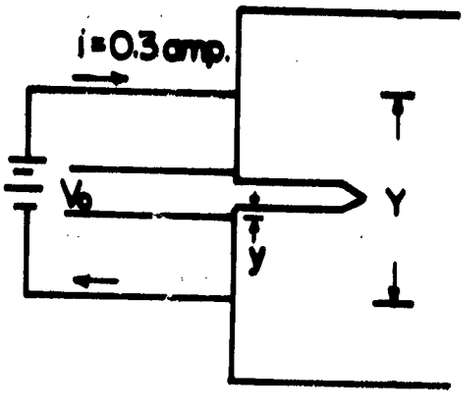

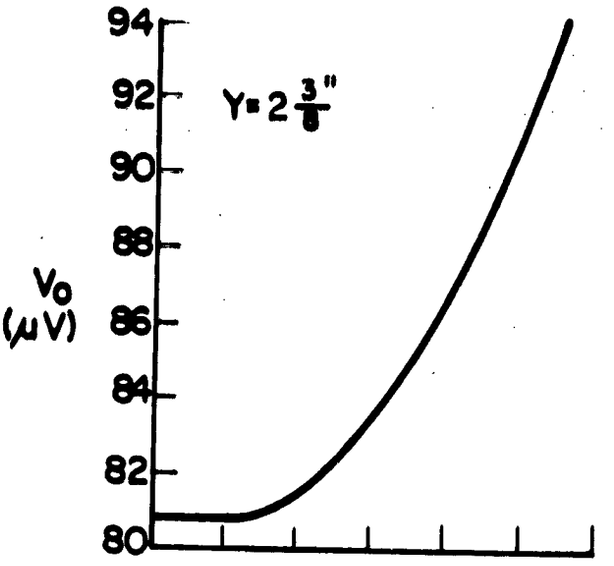

(a)

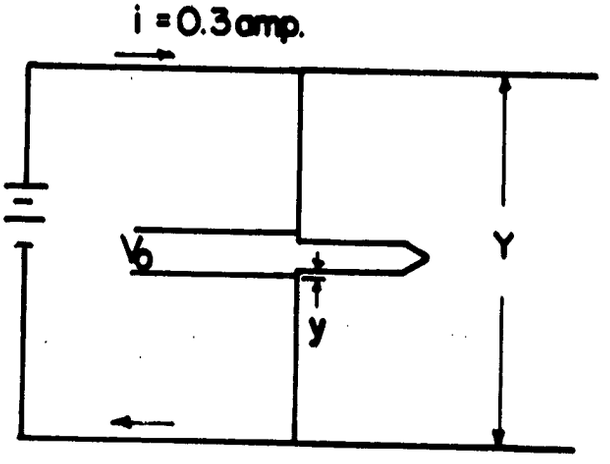

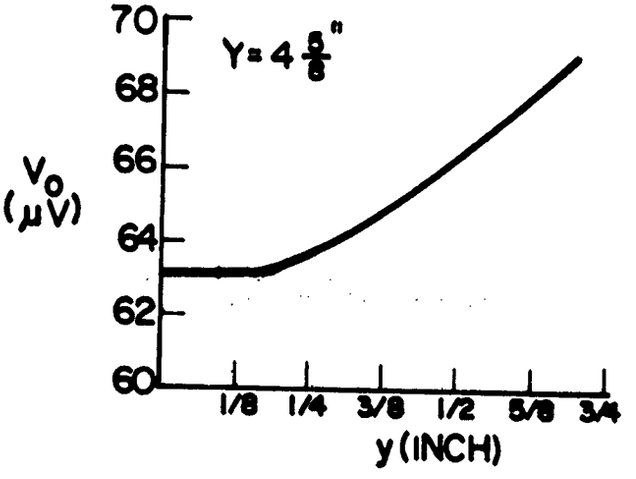

(b)

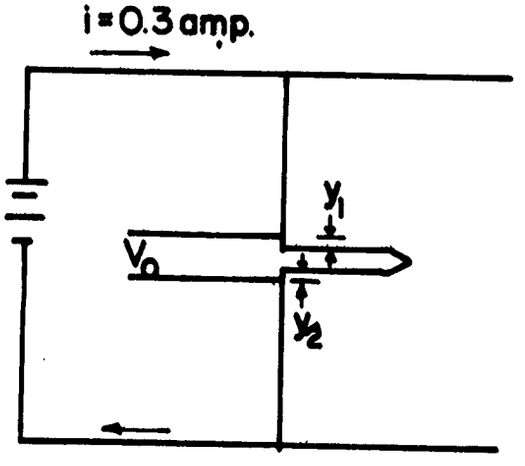

y_1 (INCH)	y_2 (INCH)	V_o(μ V)
0	1/16	63.3
1/16	1/16	63.3
0	2/16	63.3
1/16	2/16	63.3
2/16	1/16	63.3
2/16	2/16	63.3

(c)

FIG. 9 EFFECT OF POSITIONS OF CURRENT LEADS AND POTENTIAL PROBES ON POTENTIAL DROP ACROSS CRACK.

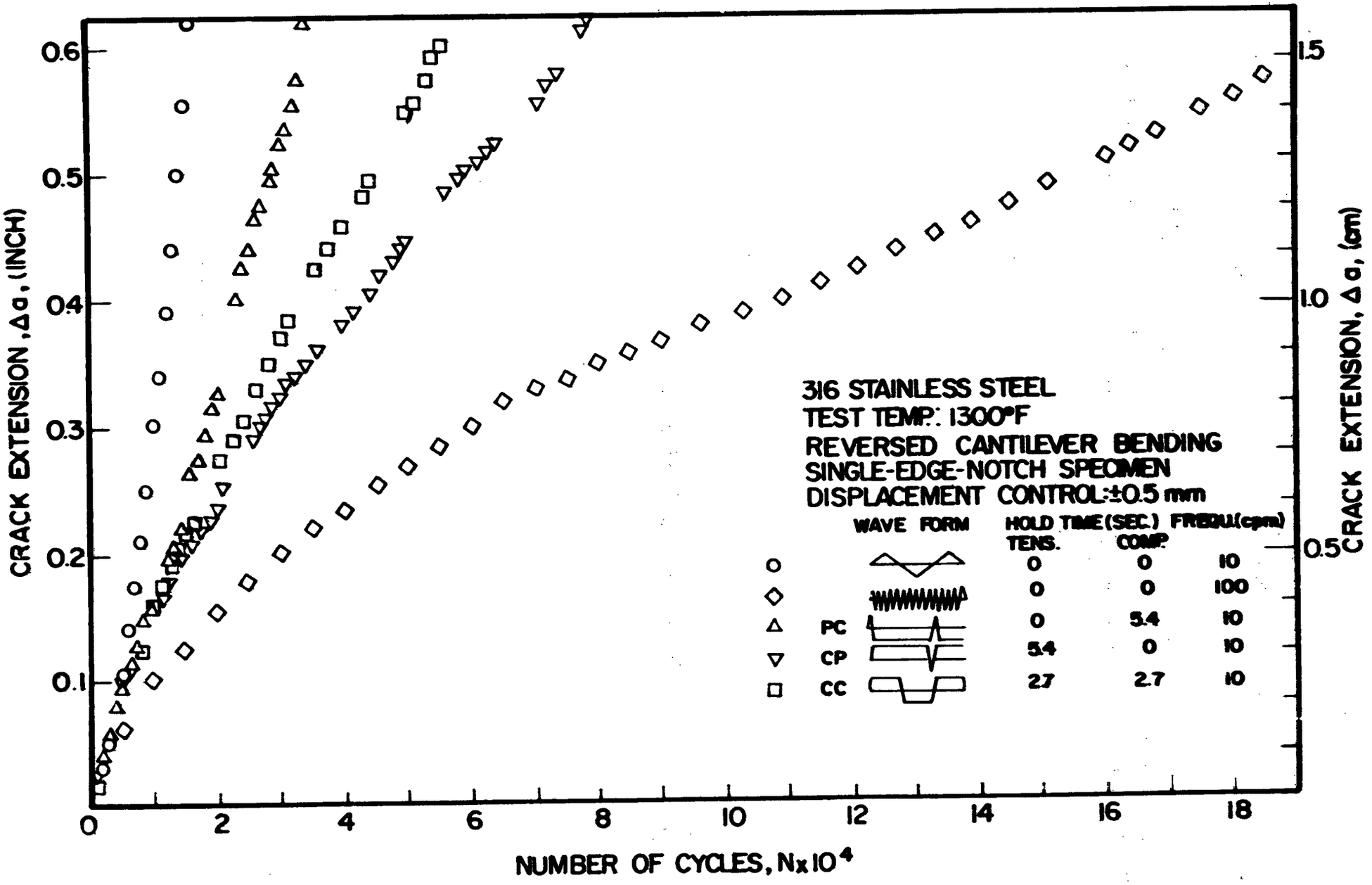

FIG. 10 CRACK GROWTH UNDER REVERSED BENDING TEST; 316 STAINLESS STEEL, 1300°F.

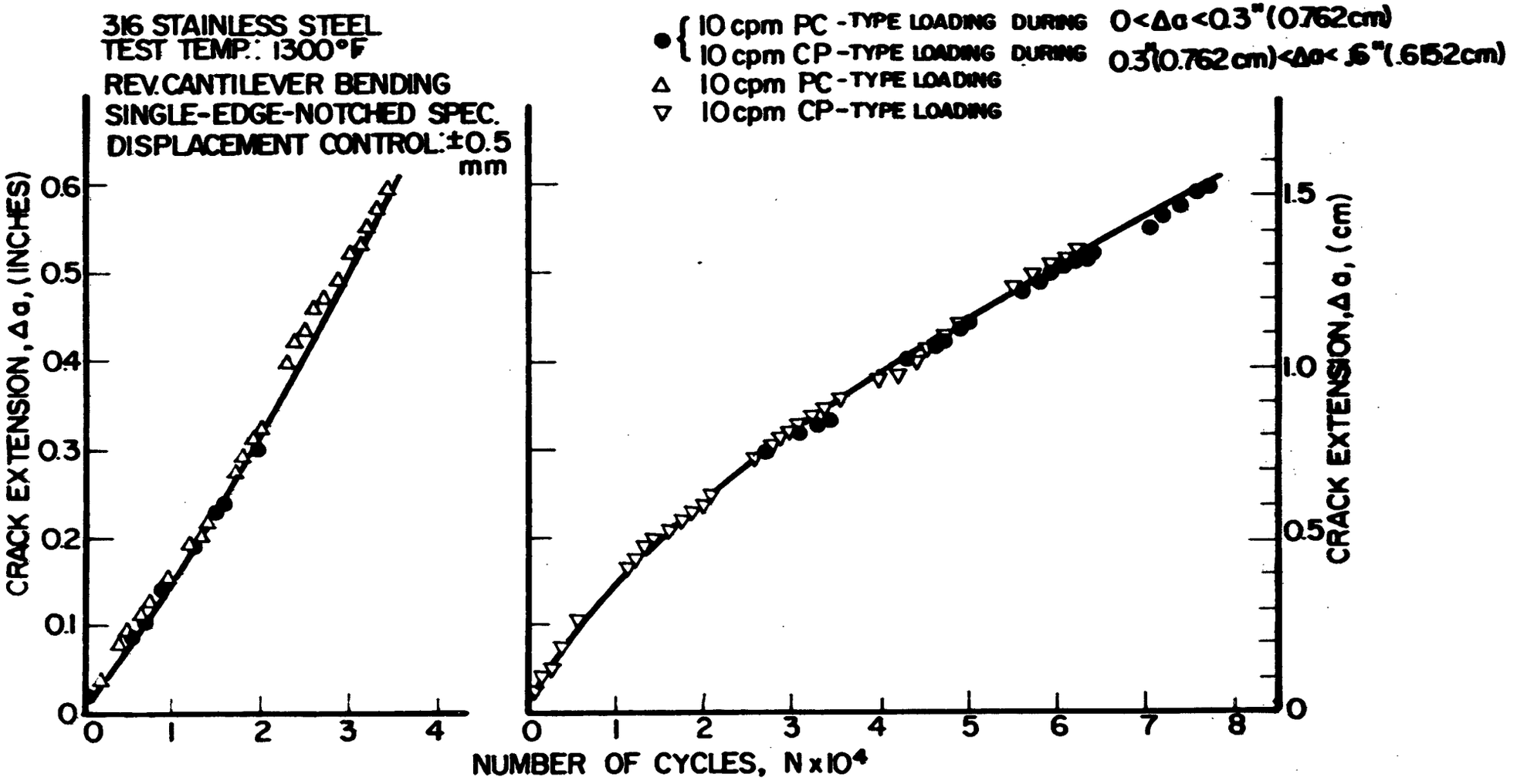

FIG. 11 CRACK GROWTH UNDER REVERSED BENDING TEST; 316 STAINLESS STEEL, 1300°F.

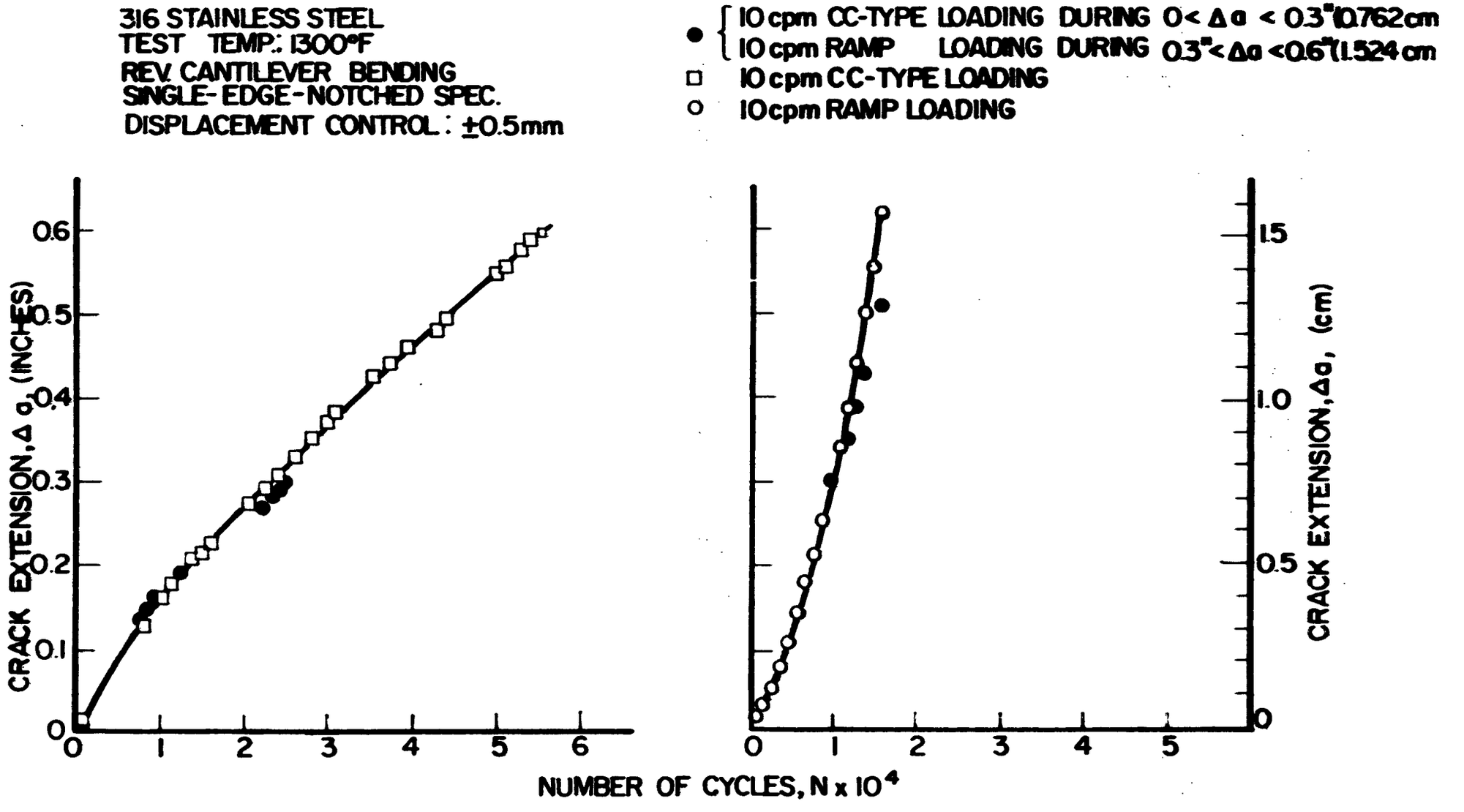

FIG. 12 CRACK GROWTH UNDER REVERSED BENDING TEST; 316 STAINLESS STEEL, 1300°F.

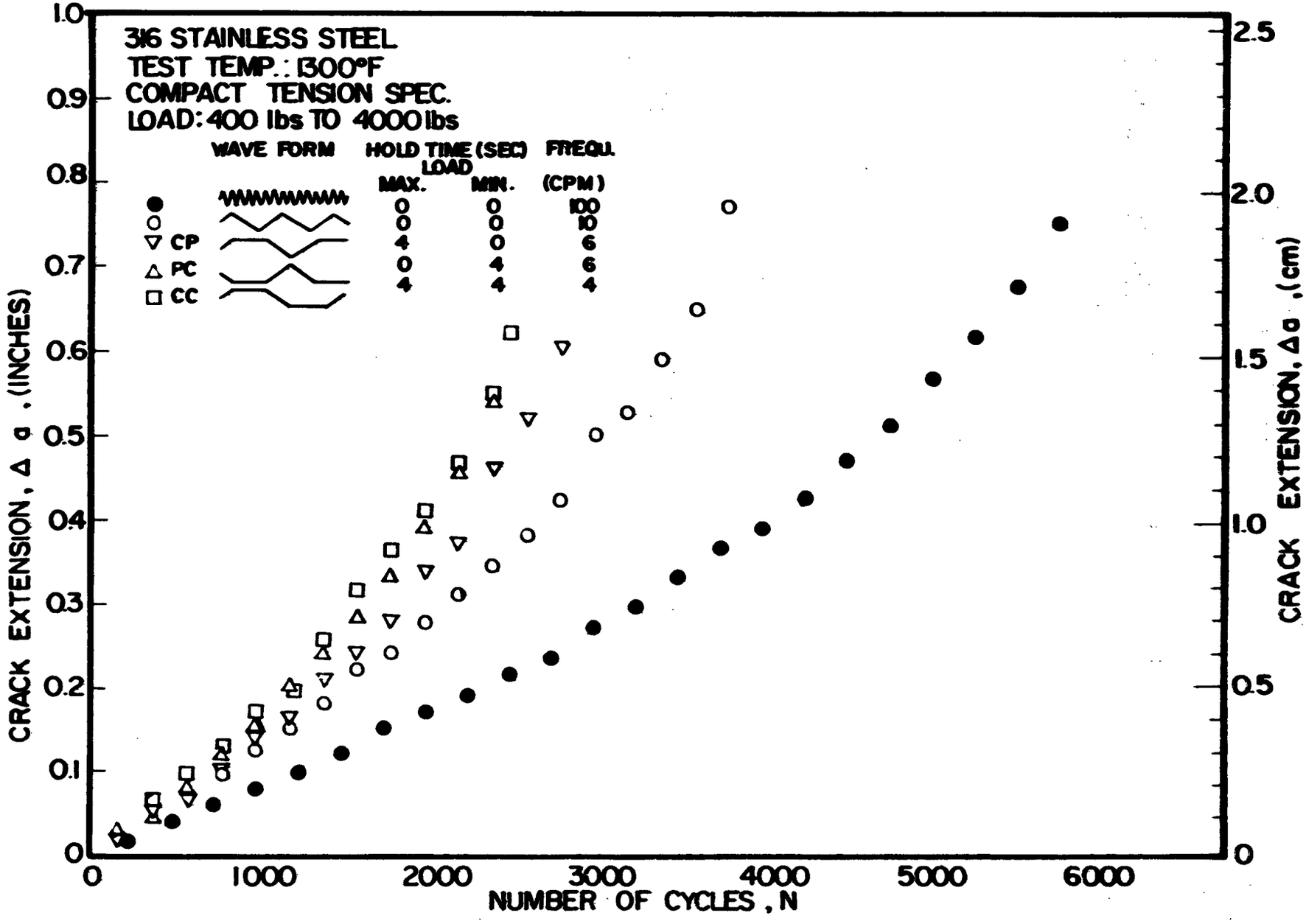

FIG. 13 CRACK GROWTH UNDER TENSION-TENSION TYPE LOADING: 316 STAINLESS STEEL, 1300°F.

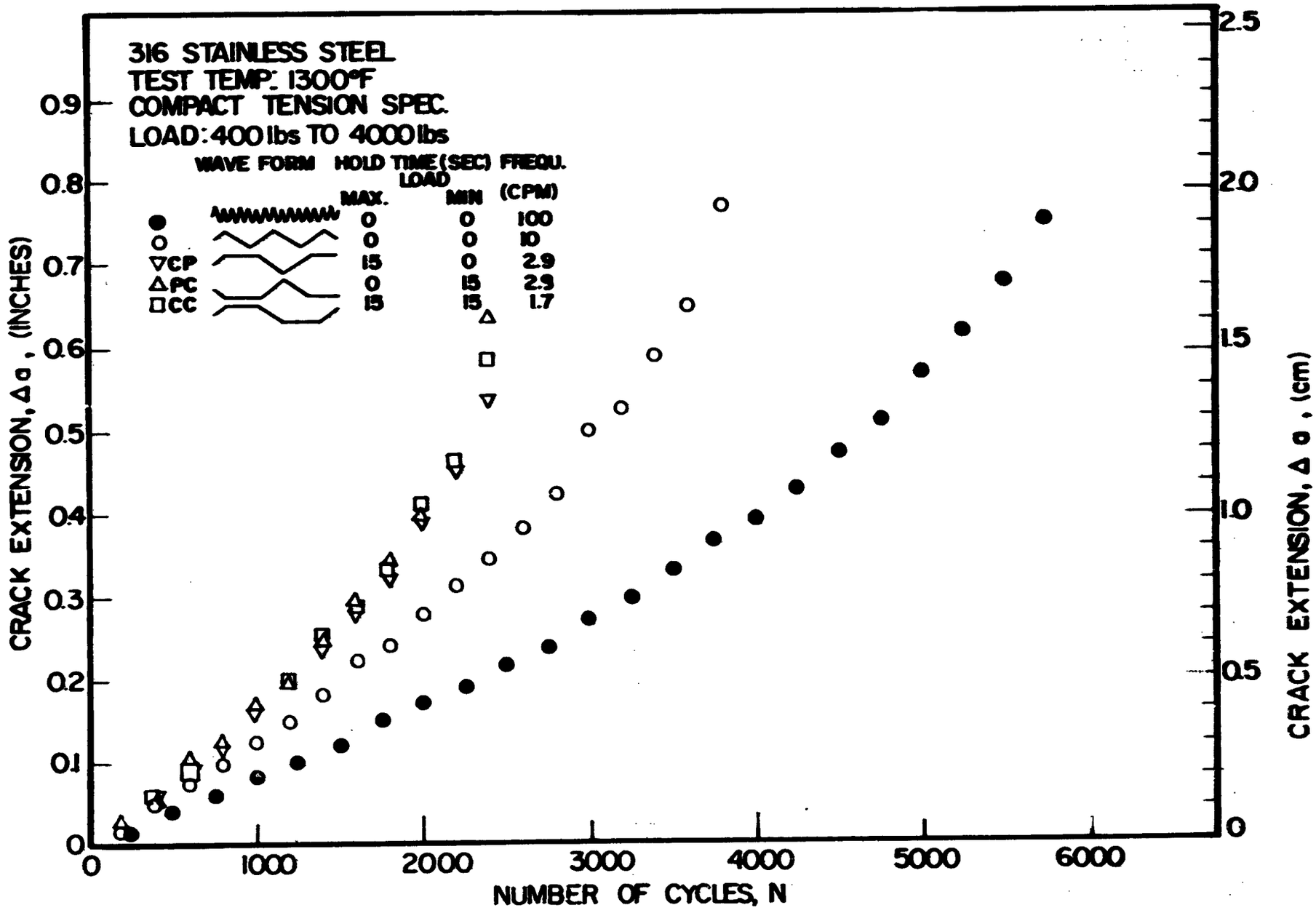

FIG. 14 CRACK GROWTH UNDER TENSION-TENSION TYPE LOADING; 316 STAINLESS STEEL, 1300°F.

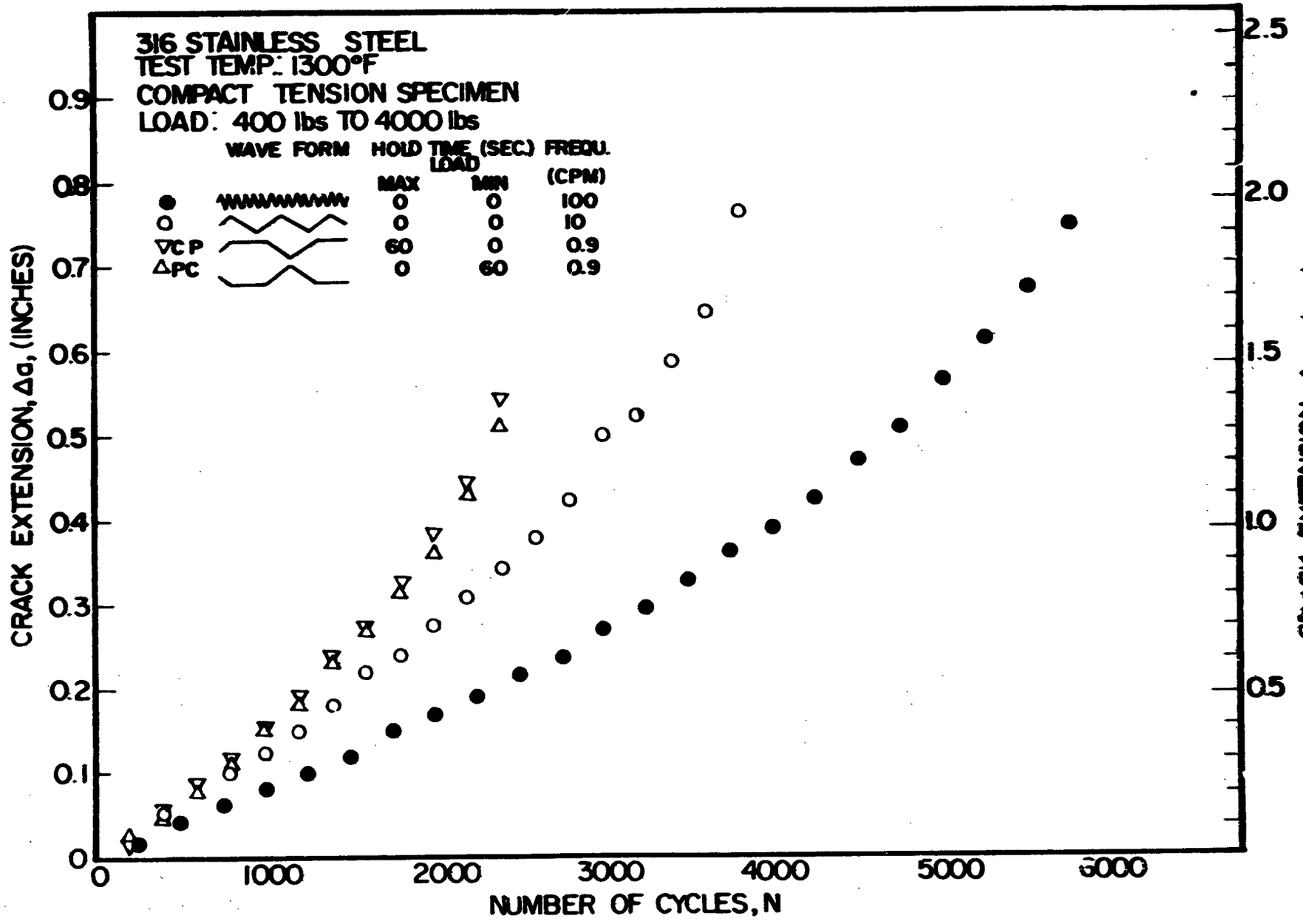

FIG. 15 CRACK GROWTH UNDER TENSION-TENSION SYM LOADING: 316 STAINLESS STEEL, 1300°F.

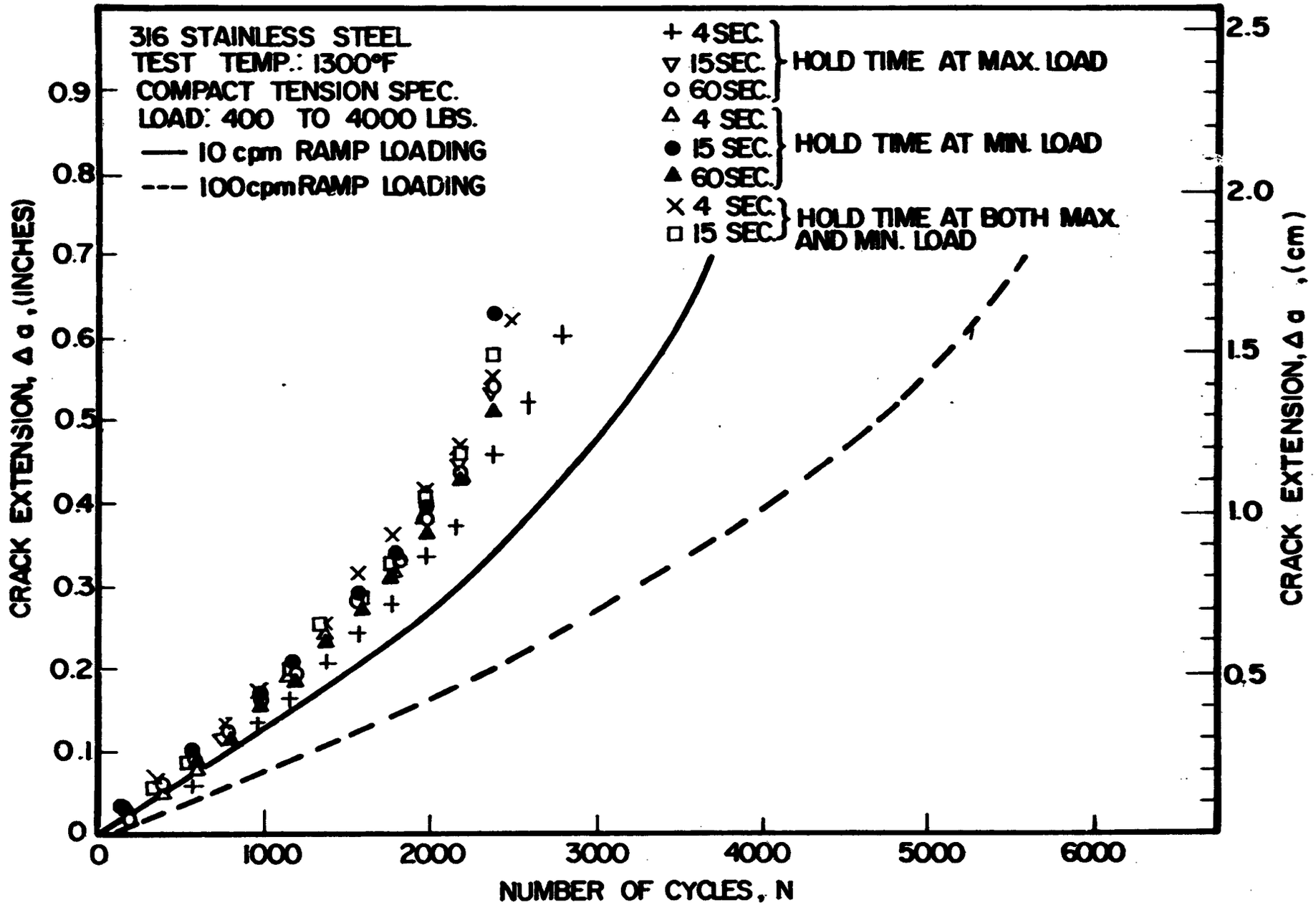

FIG. 16 SUMMARY OF CRACK GROWTH UNDER TENSION-TENSION TYPE LOADING; 316 STAINLESS STEEL, 1300°F.

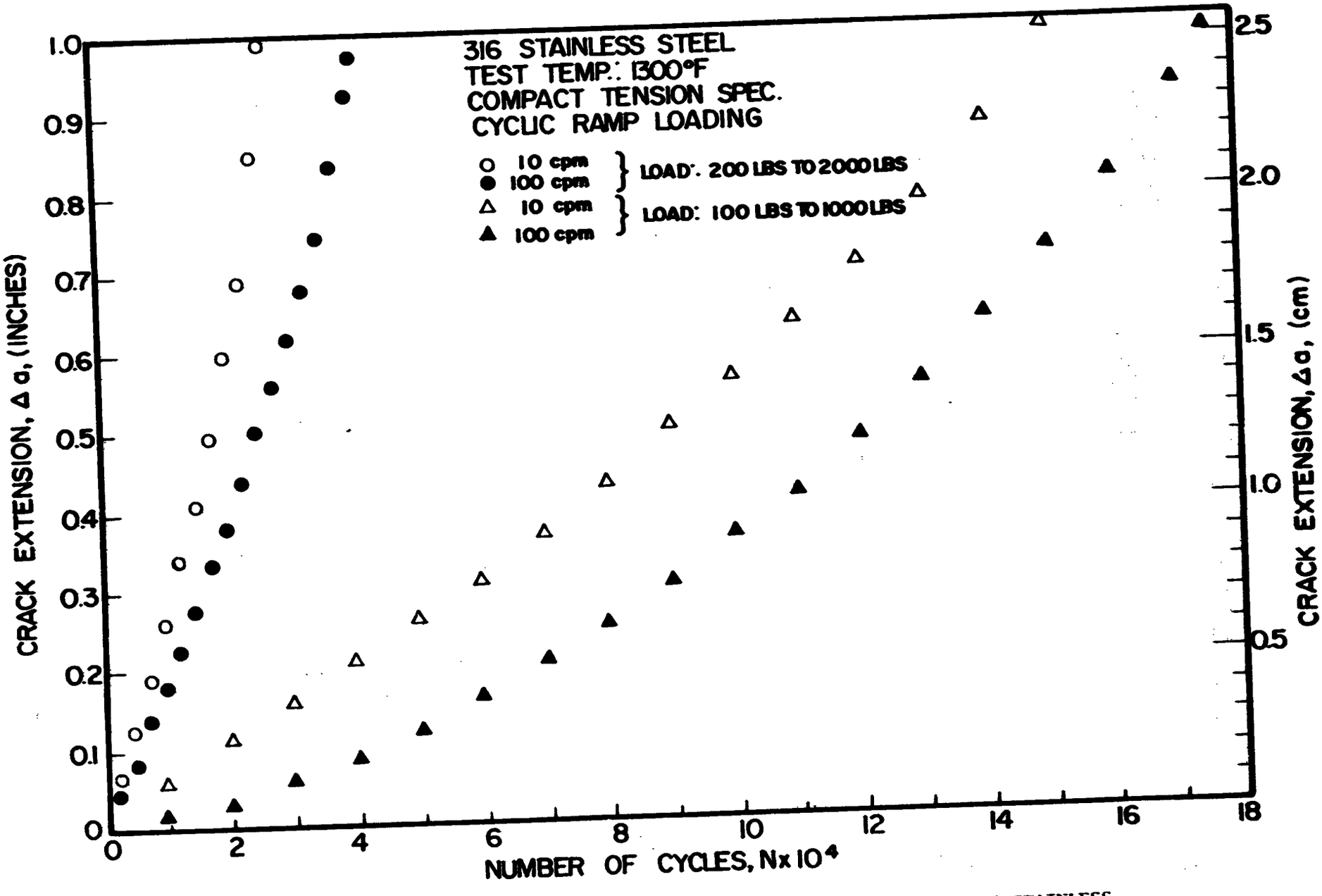

FIG. 17 CRACK GROWTH UNDER TENSION-TENSION TYPE LOADING: 316 STAINLESS STEEL, 1300°F.

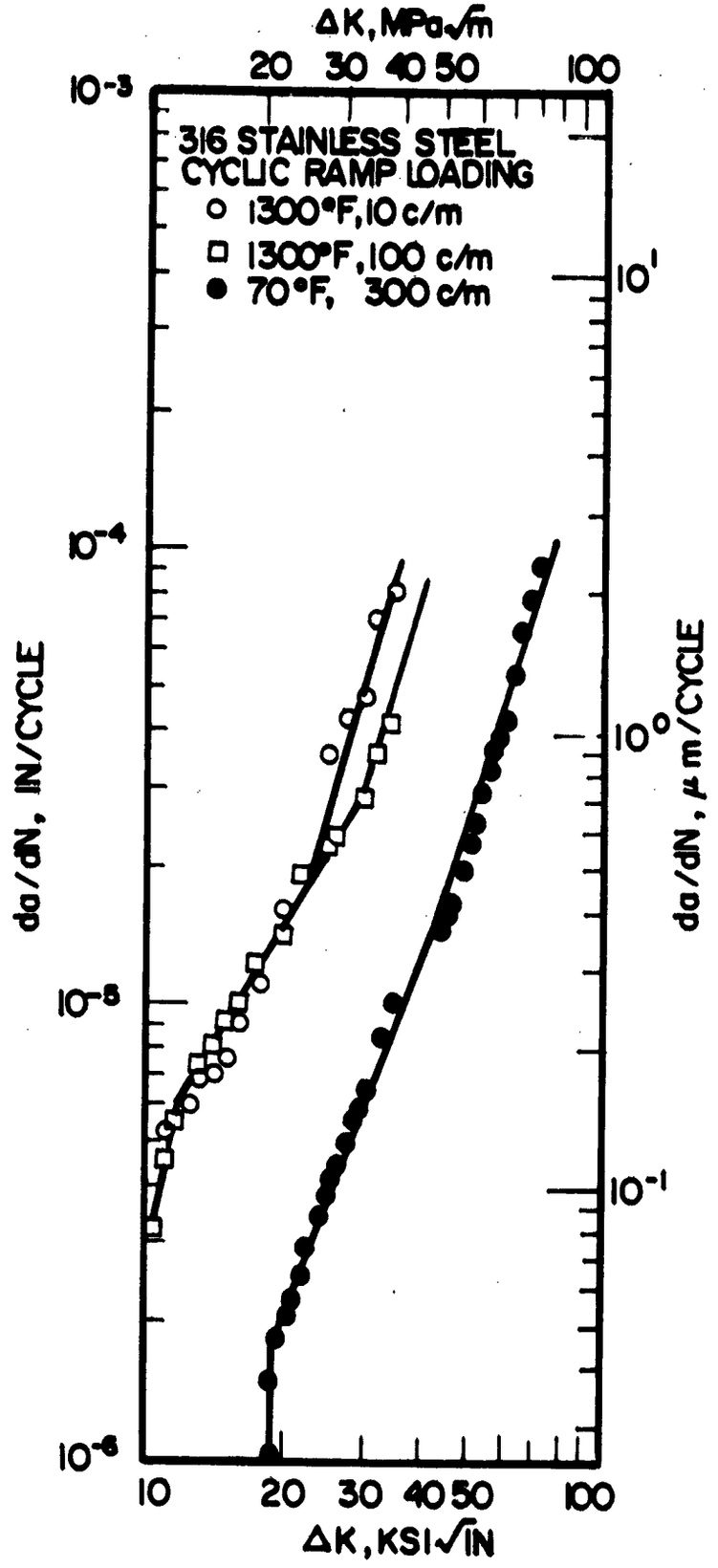

FIG. 18 CRACK GROWTH RATE VS. STRESS INTENSITY FACTOR RANGE, 316 STAINLESS STEEL.

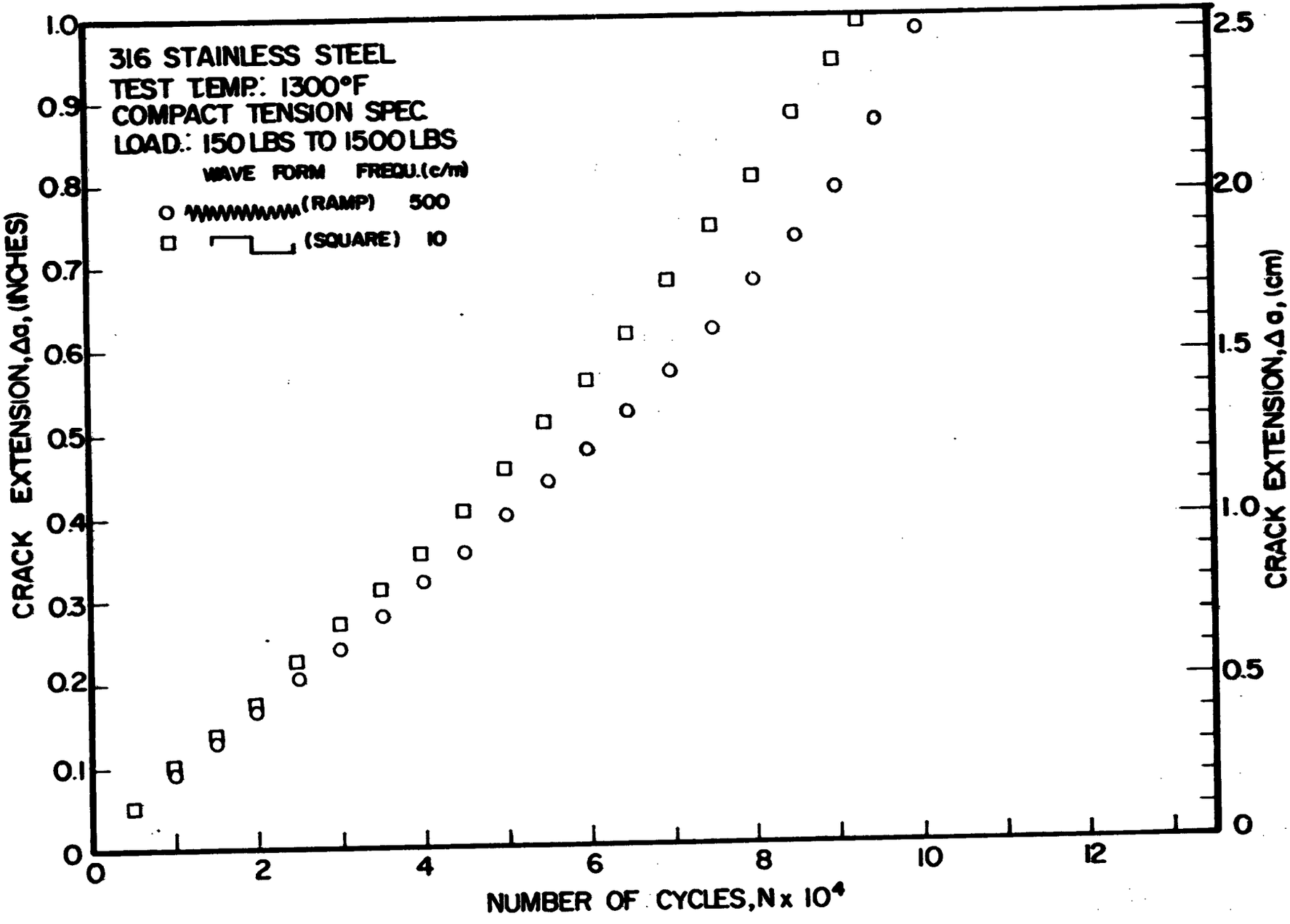

FIG. 19 CRACK GROWTH UNDER TENSION-TENSION TYPE LOADING; 316 STAINLESS STEEL, 1300°F.

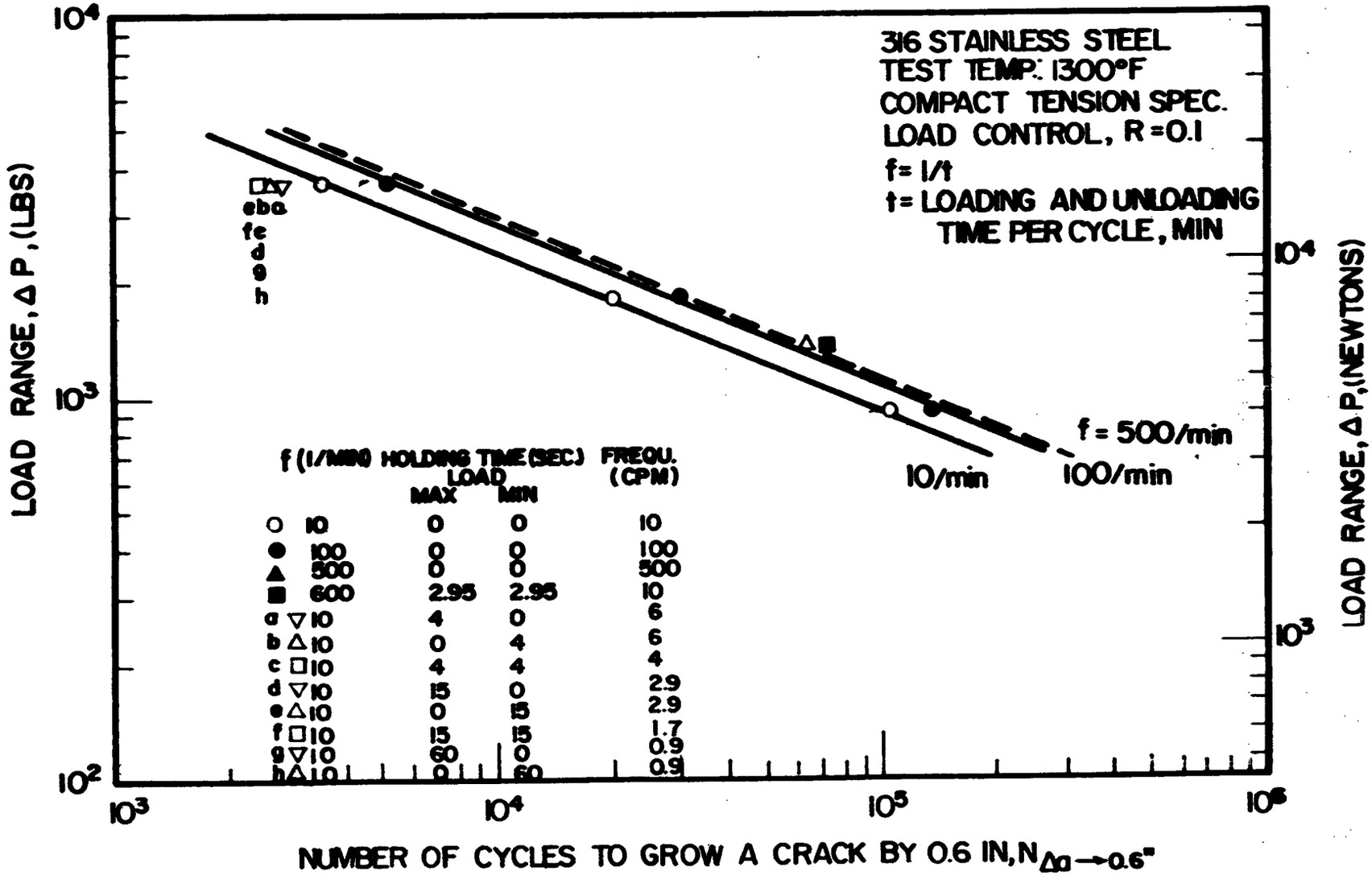

FIG. 20 LOAD RANGE VS. NUMBER OF CYCLES TO GROW A CRACK BY 0.6" FOR 316 STAINLESS STEEL AT 1300°F.

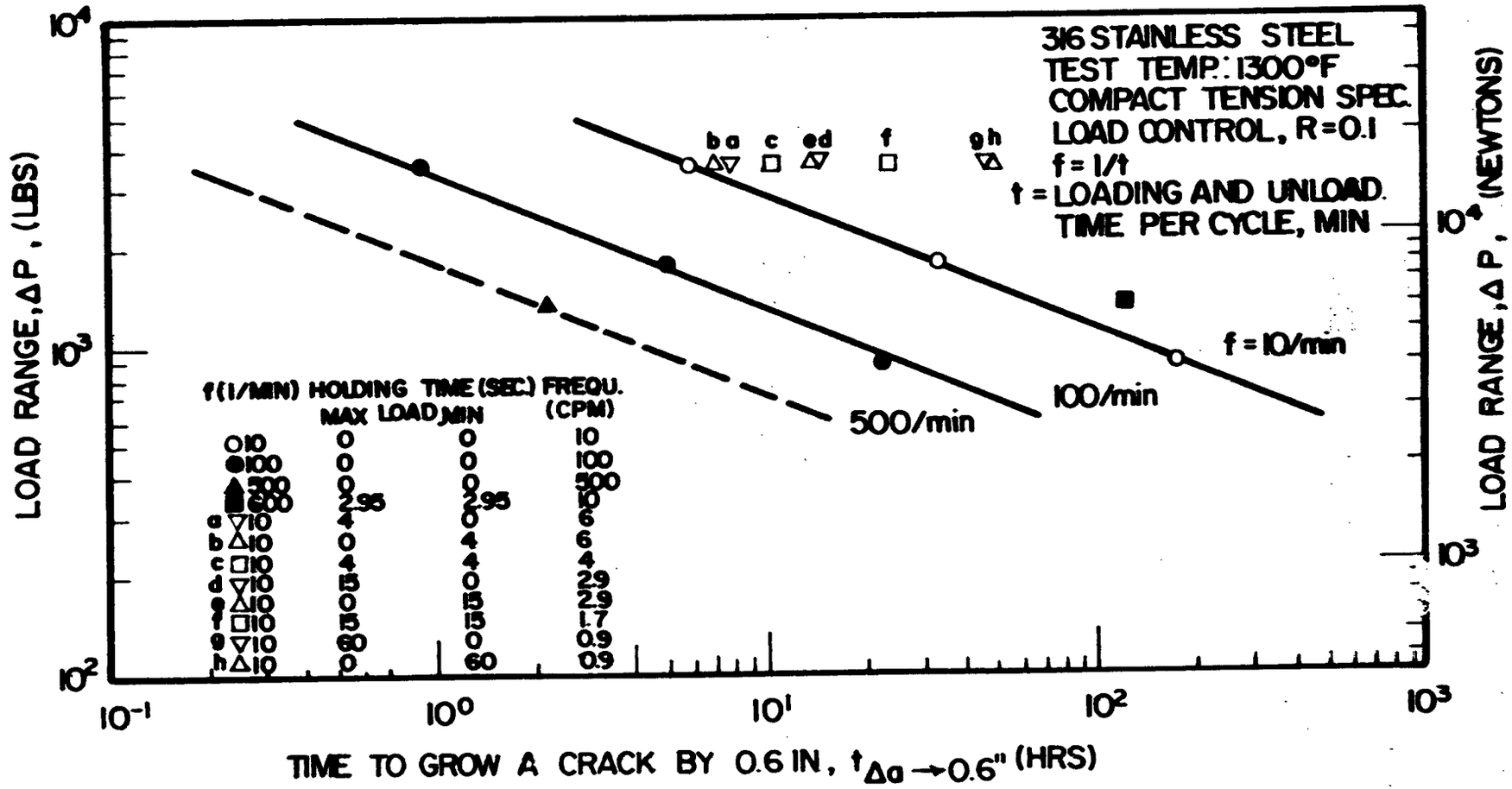

FIG. 21 LOAD RANGE VS. TIME TO GROW A CRACK BY 0.6" FOR 316 STAINLESS STEEL AT 1300°F.

(a) At notch root.

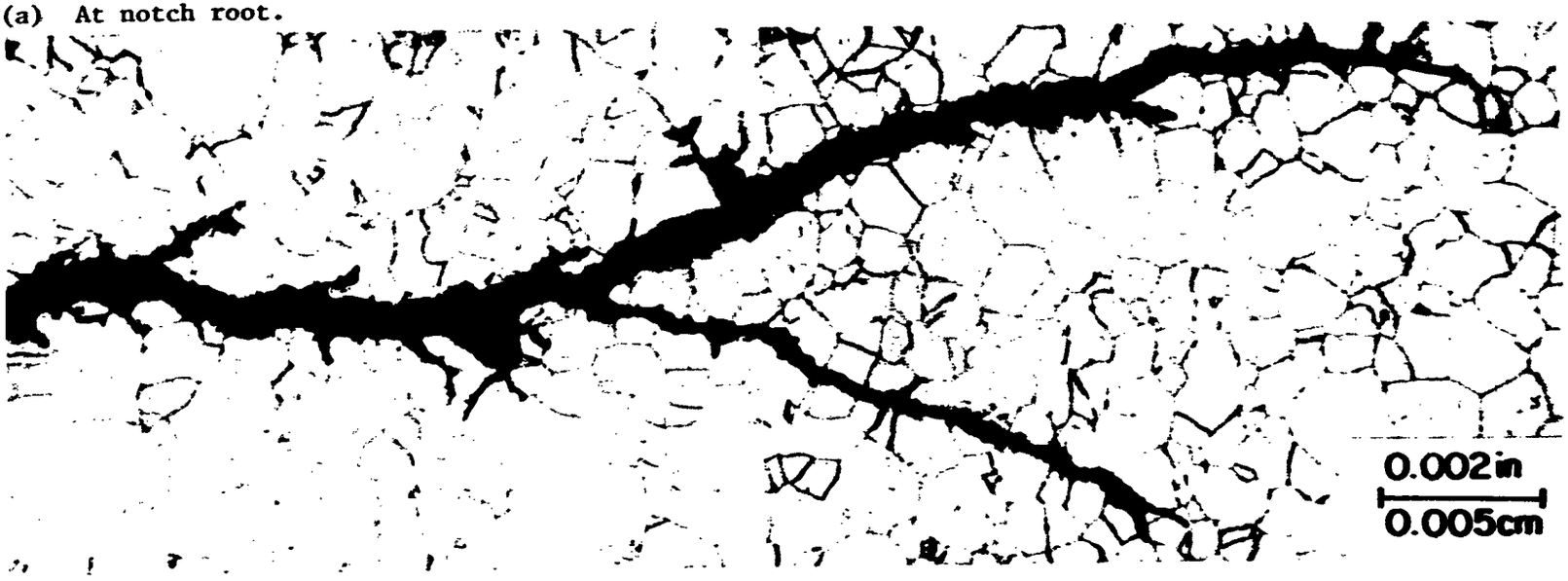

(b) At crack tip.

FIG. 22 CRACK PATH IN SEN REVERSED BENDING SPECIMEN UNDER 10 cpm RAMP LOADING; 316 STAINLESS STEEL, 1300°F. ELECTROLYTIC ETCHING: 10 ml H_2SO_4, 90 ml H_2O, 2 g CrO_3.

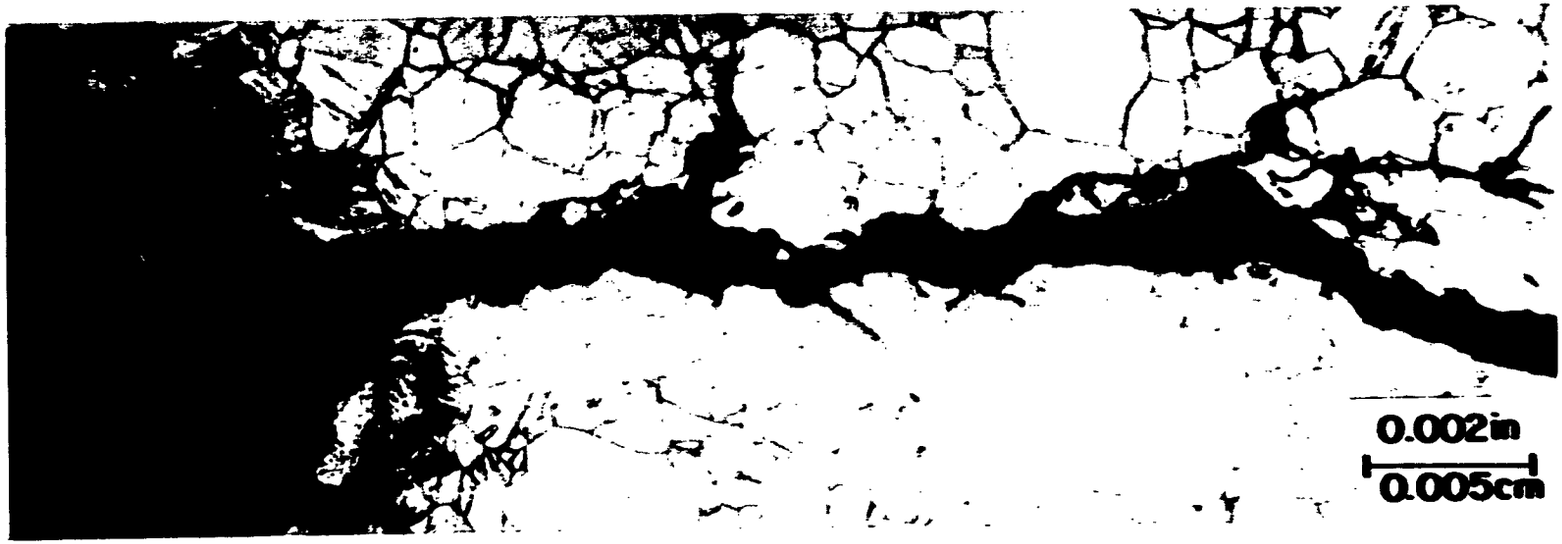

(a) At notch root.

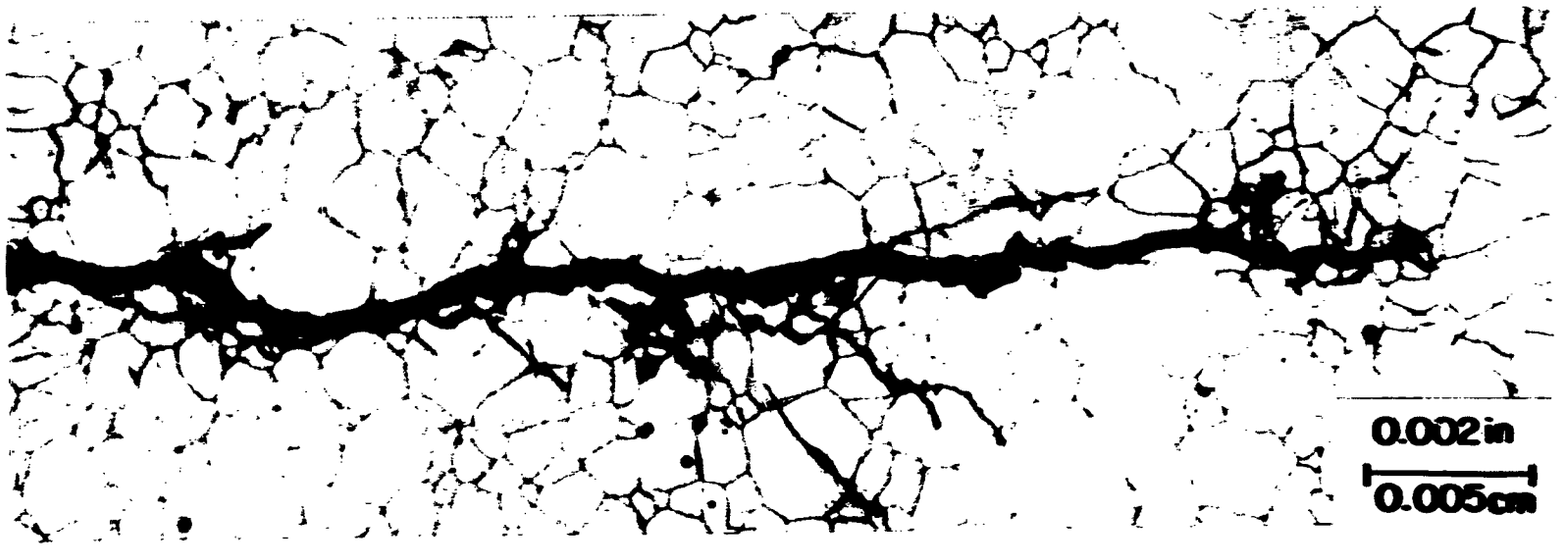

(b) At crack tip.

FIG. 23 CRACK PATH IN SEN REVERSED BENDING SPECIMEN UNDER 10 cpm pc-TYPE LOADING; 316 STAINLESS STEEL, 1300°F. ELECTROLYTIC ETCHING: 10 ml H_2SO_4, 90 ml.H_2O, 2 g CrO_3.

(a) At notch root.

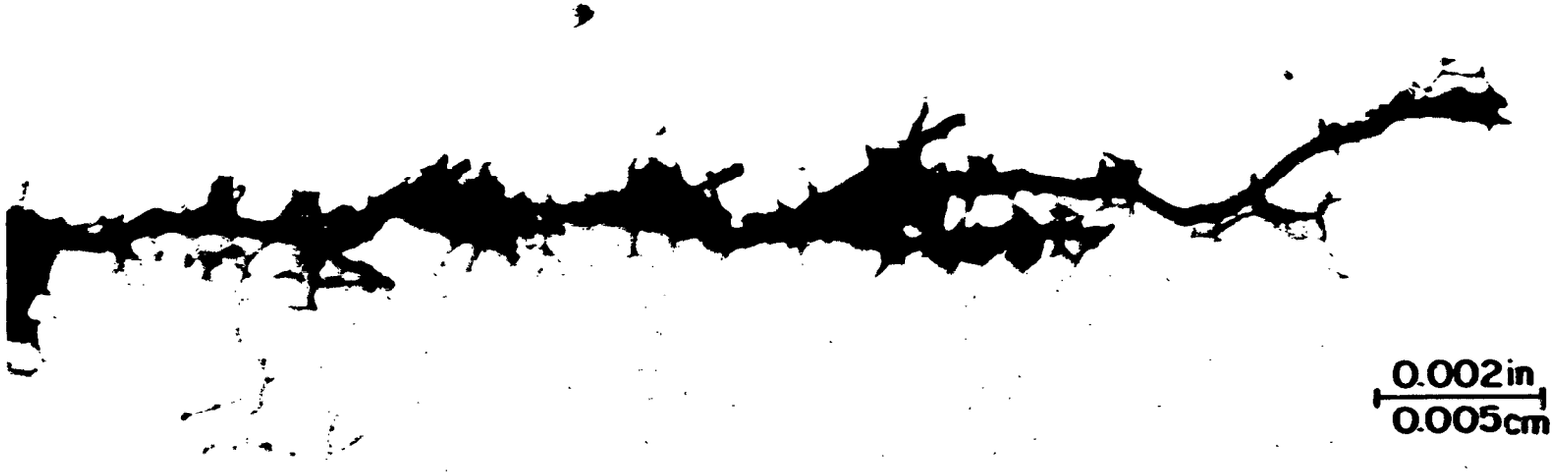

(b) At crack tip.

FIG. 24 CRACK PATH IN SEN REVERSED BENDING SPECIMEN UNDER 10 cpm cc-TYPE LOADING; 316 STAINLESS STEEL, 1300°F. ELECTROLYTIC ETCHING: 10 ml H_2SO_4, 90 ml H_2O, 2 g CrO_3.

(a) At notch root.

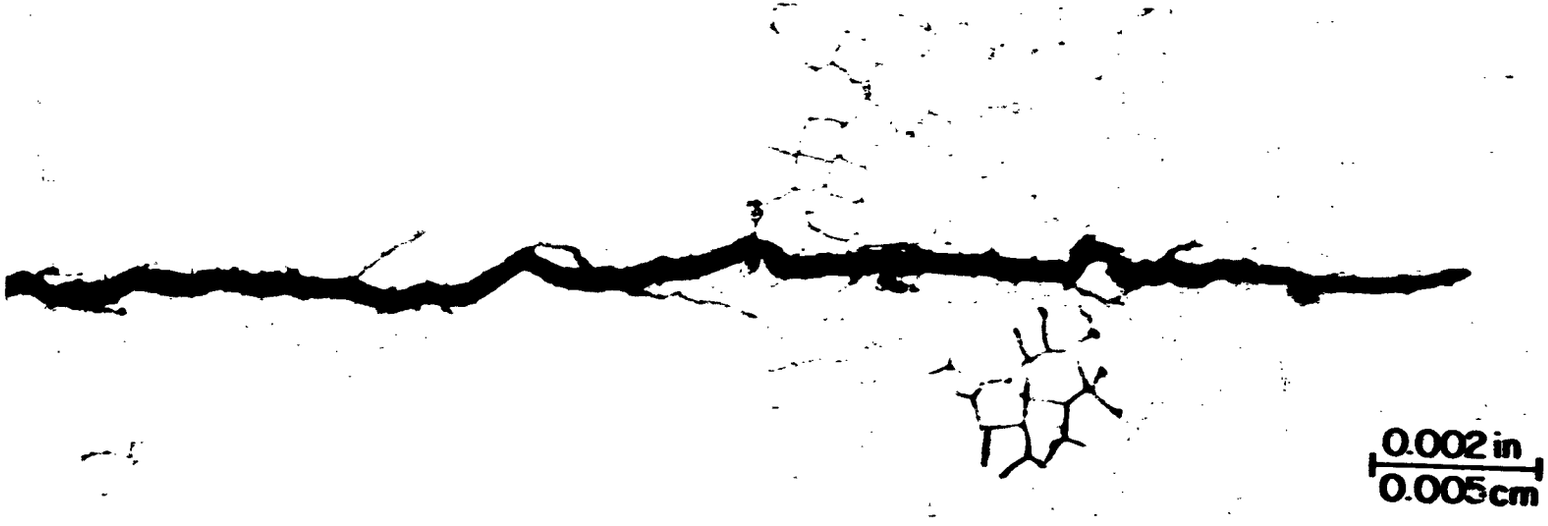

(b) At crack tip.

FIG. 25 CRACK PATH IN SEN REVERSED BENDING SPECIMEN UNDER 10 cpm cp-TYPE LOADING; 316 STAINLESS STEEL, 1300°F. ELECTROLYTIC ETCHING: 10 ml H_2SO_4, 90 ml H_2O, 2 g CrO_3.

(a) At notch root.

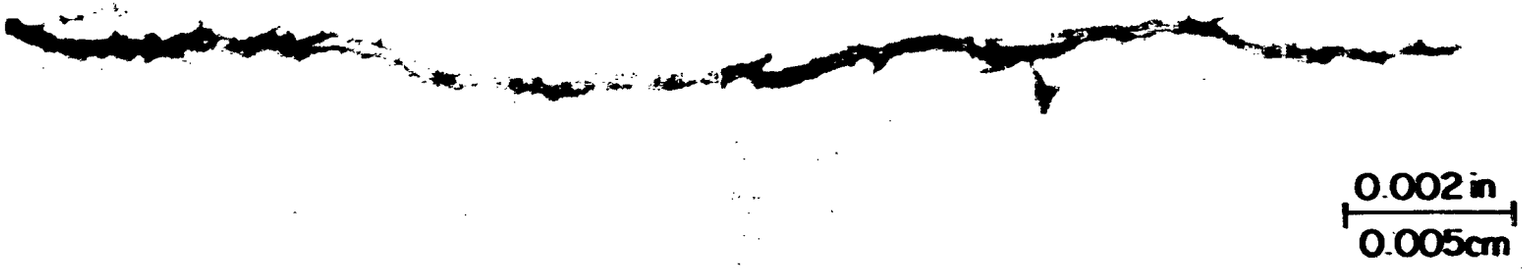

(b) At crack tip.

FIG. 26 CRACK PATH IN SEN REVERSED BENDING SPECIMEN UNDER 100 cpm RAMP LOADING: 316 STAINLESS STEEL, 1300°F. ELECTROLYTIC ETCHING: 10 ml H_2SO_4, 90 ml H_2O, 2 g CrO_3.

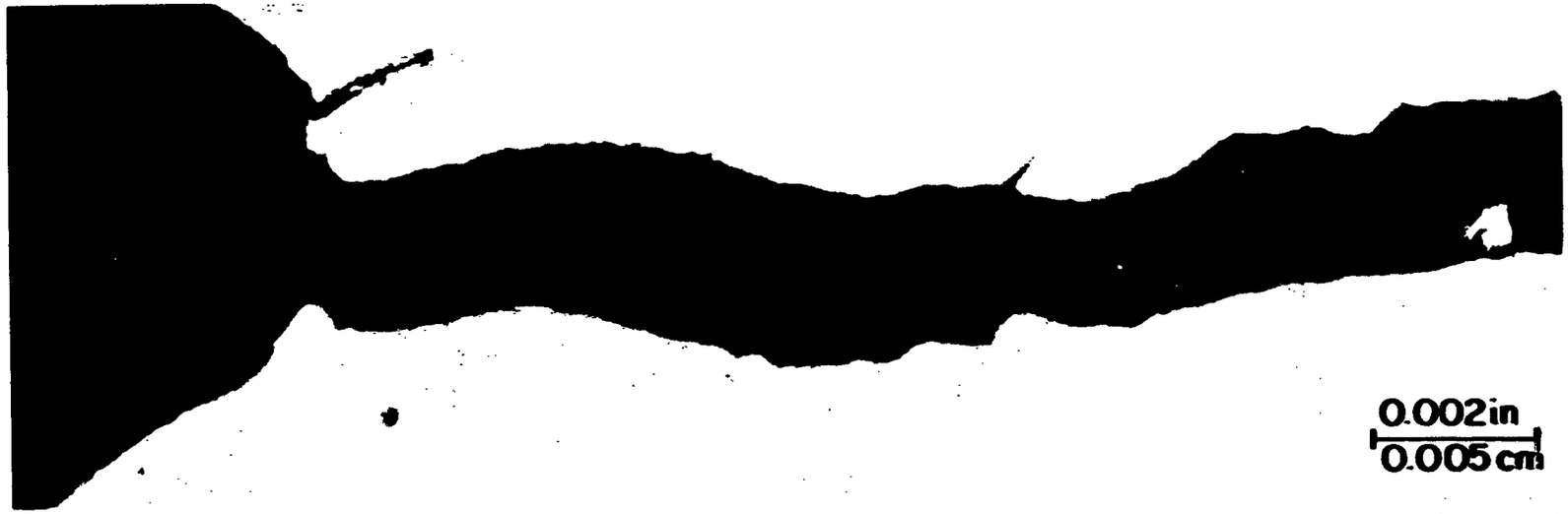

(a) At notch root.

(b) At crack tip.

FIG. 27 CRACK PATH IN COMPACT TENSION SPECIMEN UNDER 10 cpm RAMP LOADING (LOAD: 200 to 2000 LBS.); 316 STAINLESS STEEL, 1300°F. ELECTROLYTIC ETCHING: 10 ml H_2SO_4, 90 ml H_2O, 2 g CrO_3.

(a) At notch root.

(b) At crack tip.

FIG. 28 CRACK PATH IN COMPACT TENSION SPECIMEN UNDER 100 cps RAMP LOADING (LOAD: 200 to 2000 LBS.); 316 STAINLESS STEEL, 1300°F. ELECTROLYTIC ETCHING: 10 ml H_2SO_4, 90 ml H_2O, 2 g CrO_3.

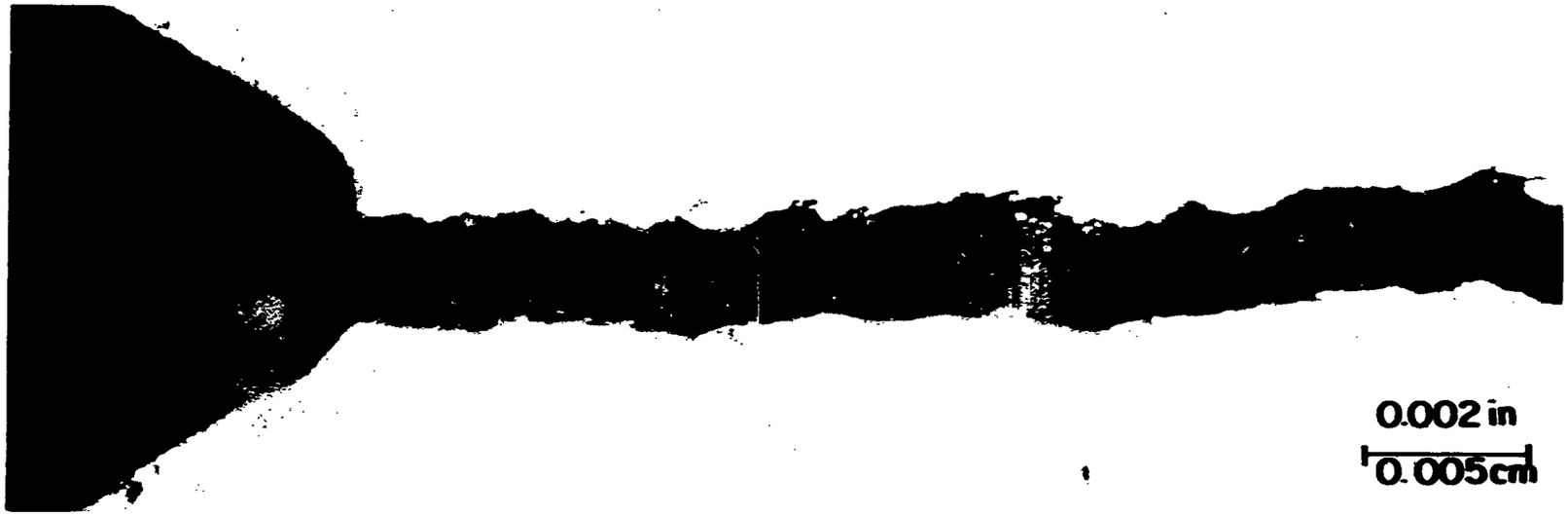

(a) At notch root.

(b) At crack tip.

FIG. 29 CRACK PATH IN COMPACT TENSION SPECIMEN UNDER 500 cpm RAMP LOADING (LOAD: 150 to 1500 LBS.); 316 STAINLESS STEEL, 1300°F. ELECTROLYTIC ETCHING: 10 ml H_2SO_4, 90 ml H_2O, 2 g CrO_3.

(a) At notch root.

(b) At crack tip.

FIG. 30 CRACK PATH IN COMPACT TENSION SPECIMEN UNDER 10 cpm SQUARE WAVE FORM LOADING (LOAD: 150 to 1500 LBS.);316 STAINLESS STEEL, 1300°F. ELECTROLYTIC ETCHING: 10 ml H_2SO_4, 90 ml H_2O, 2 g CrO_3.

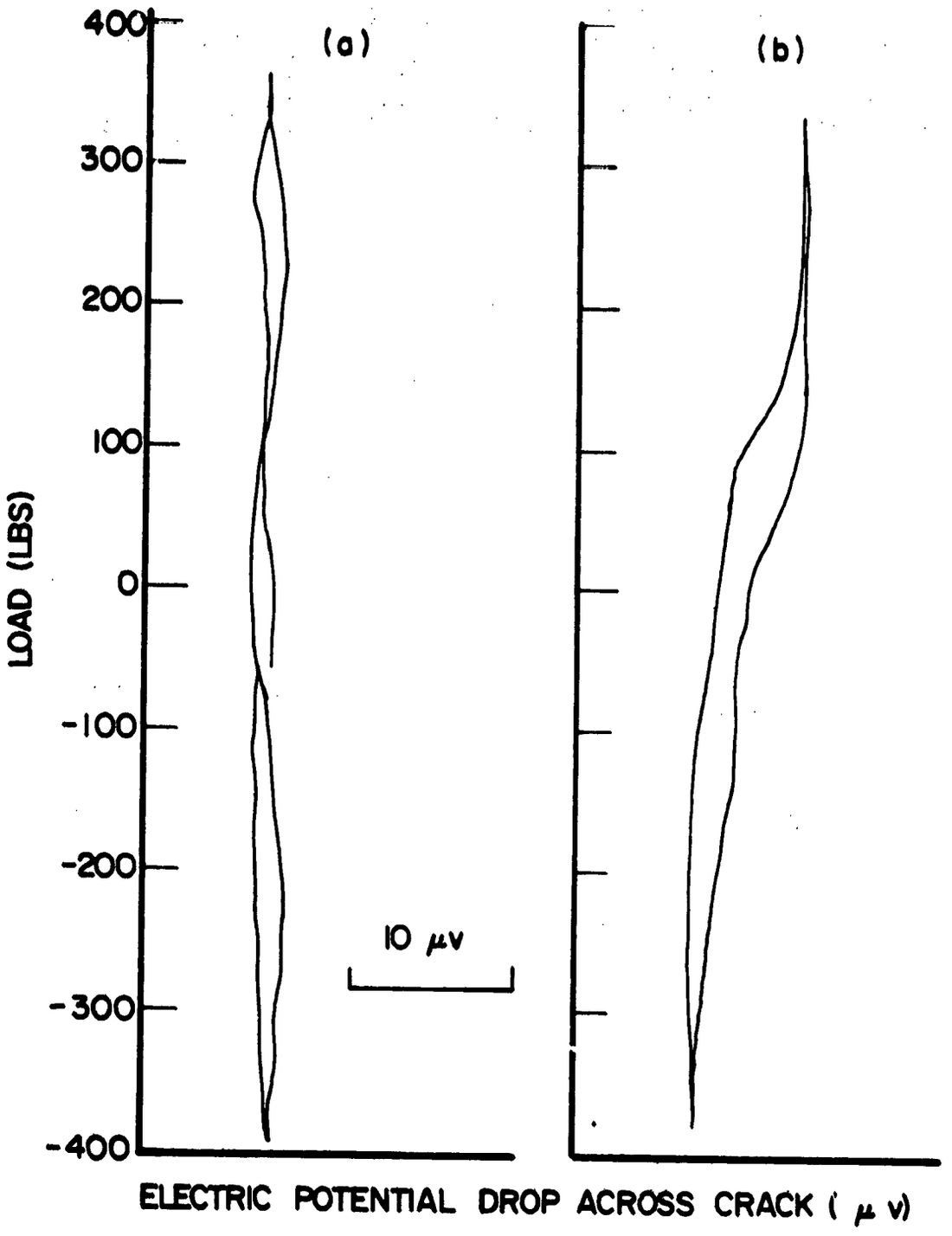

FIG. 31 TRACING OF LOAD VS. ELECTRIC POTENTIAL DROP FOR (a) 10 cpm AND (b) 100 cpm RAMP-TYPE REVERSED BENDING; 316 STAINLESS STEEL, 1300°F.

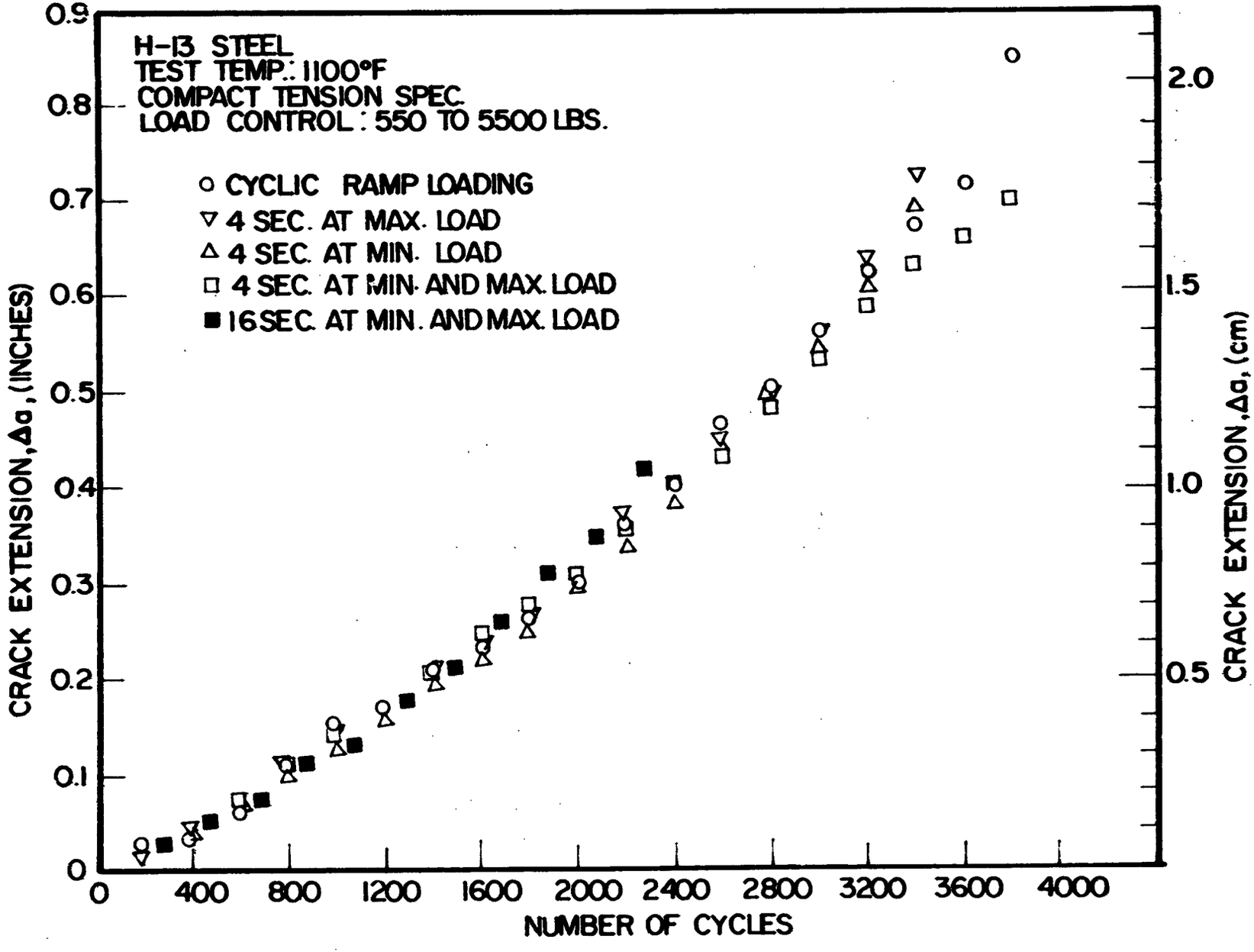

FIG. 32 CRACK GROWTH UNDER TENSION-TENSION TYPE LOADING: H-13 STEEL, 1100°F.